Role of feedback and dynamics in a gene regulatory network

Thesis by

Ophelia S. Venturelli

In Partial Fulfillment of the Requirements

for the Degree of

Doctor of Philosophy

California Institute of Technology

Pasadena, California

2013

(Defended May 30, 2013)

Acknowledgements

I am very fortunate to have had the opportunity of attending Caltech for graduate school. I appreciate many unique characteristics of Caltech including an intimate community where I can walk around campus and recognize many familiar faces, a relaxed yet challenging and stimulating intellectual environment and the absence of barriers for interdisciplinary research. I also had the privilege of spending almost two years at UCSF during my graduate studies. UCSF is a cutting-edge and exciting place to work and I have learned a tremendous amount during my tenure at UCSF.

I would like to especially thank my advisor Richard Murray for his guidance, support and for allowing me the freedom to explore interesting scientific questions. Richard has an incredible positive energy and enthusiasm that has reinforced my motivation about science over the years. By working with Richard, I have learned a quantitative and rigorous reasoning about biological systems. I have enjoyed interacting with members of the Murray group and appreciate their diverse backgrounds in math, computer science, engineering and biology.

I am most grateful to Hana El-Samad, who has been a second advisor to me, for the opportunity to pursue exciting research projects in her lab and for supporting my research. Hana is very detail-oriented and meticulous about scientific research and as a consequence I think my approach to scientific problems and writing has significantly improved. Hana also has excellent intuition for how to tie together a set of data to tell a compelling scientific story. Finally, Hana provided me with an enjoyable and intellectually stimulating environment. I have learned many lessons in her lab that will be indispensable for my future scientific career.

I would like to credit many colleagues at both Caltech and UCSF for their guidance, support and scientific feedback. I would like to especially recognize Ignacio Zuleta for our productive collaboration. I have greatly benefited from countless scientific discussions with Fiona Chandra, Elisa Franco and Marcella Gomez. I am appreciative for Andrés Aranda's help in the lab. My research has significantly benefited from my collaboration with Adam Rosenthal. I am thankful to David Soloveichik for helping me to think differently about theoretical research problems. Richard's group recently exhibited an period of exponential growth and I would like to thank the new members of his lab including Dan Siegal-Gaskins, Anu Thubagere, Jongmin Kim, Nadine Dabby, Emzo de los Santos, Joe Meyerowitz, Enoch Yeung and Vanessa Jönsson. Finally, I would like to extend my appreciation to other members of Hana's lab including Benjamin Heineike, Raj Bhatnagar, Michael Chevalier, Joanna Lipinski-Kruszka, Susan Chen, Patrick Harrigan and Graham Heimberg.

I am especially grateful to my committee including Michael Elowitz, Rob Phillips and Raymond Deshaies for providing valuable feedback. In particular, I am indebted to Michael Elowitz who allowed me to participate in his lab's group meetings and provide excellent scientific guidance. Michael's approach to biology has been an inspiration for my graduate work. I am thankful to Steve Mayo for providing me with lab space at Caltech.

I would like to recognize the Biochemistry and Molecular Biophysics (BMB) graduate program and especially thank Allison Ross and Doug Rees in organizing this program and supporting graduate students.

I would not be where I am today without the love and support of my family. My parents, Shalini and Peter Venturelli have provided me with unconditional support and I would like to thank them for always believing in me. My brother, Philip Venturelli, instilled in me a deep scientific curiosity. I am obliged to Louis and Shelley Romero for their assistance during my graduate studies. In

particular, my research has benefited significantly from many instructive conversations with Louis Romero about math and dynamical systems. It has been really fun to share my graduate experiences with my husband, Philip Romero. Philip's scientific feedback and support has been invaluable.

Abstract

Cells exhibit a diverse repertoire of dynamic behaviors. These dynamic functions are implemented by circuits of interacting biomolecules. Although these regulatory networks function deterministically by executing specific programs in response to extracellular signals, molecular interactions are inherently governed by stochastic fluctuations. This molecular noise can manifest as cell-to-cell phenotypic heterogeneity in a well-mixed environment. Single-cell variability may seem like a design flaw but the coexistence of diverse phenotypes in an isogenic population of cells can also serve a biological function by increasing the probability of survival of individual cells upon an abrupt change in environmental conditions. Decades of extensive molecular and biochemical characterization have revealed the connectivity and mechanisms that constitute regulatory networks. We are now confronted with the challenge of integrating this information to link the structure of these circuits to systems-level properties such as cellular decision making. To investigate cellular decision-making, we used the well studied galactose gene-regulatory network in *Saccharomyces cerevisiae*. We analyzed the mechanism and dynamics of the coexistence of two stable on and off states for pathway activity. We demonstrate that this bimodality in the pathway activity originates from two positive feedback loops that trigger bistability in the network. By measuring the dynamics of single-cells in a mixed sugar environment, we observe that the bimodality in gene expression is a transient phenomenon. Our experiments indicate that early pathway activation in a cohort of cells prior to galactose metabolism can accelerate galactose consumption and provide a transient increase in growth rate. Together these results provide important insights into strategies implemented by cells that may have been evolutionary advantageous in competitive environments.

Contents

Chapter 1

Introduction

Introduction

Biological systems exhibit remarkable phenotypic diversity. The myriad of phenotypes are achieved through networks of interacting biomolecules that produce a rich repertoire of dynamical functions at the cellular level. For example, these circuits have been shown to produce oscillations, excitability, adaptive responses and bistability [1, 2, 3, 4]. Due to the discrete nature of molecular interactions, the dynamic responses are inherently stochastic and display significant fluctuations in the concentrations of components. Indeed, single microbial and eukaryotic cells can exhibit significant phenotypic heterogeneity that does not stem from a genetic origin.

Although the inescapable noise in the levels and activities of biomolecules seems undesirable for cells, previous studies have shown that phenotypic variability can be functionally beneficial in specific environments. This bet-hedging phenomenon is characterized by more than one coexisting phenotype in a uniform environment that provides a temporary disadvantage for the population but can confer a long-term fitness advantage upon an abrupt environmental change [5]. In bacteria for example, competence, sporulation, and persistence in response to high doses of antibiotics have been shown to enhance population fitness by increasing the chance of survival upon a shift in the environmental conditions [6, 7, 8]. In all of these cases, noise in the levels of critical regulatory molecules influences a binary cellular decisions. Recently, yeast have also been shown to benefit from bet-hedging strategies by diversifying the range of growth rates or displaying asymmetric

growth behaviors in response to specific stress stimuli such as metal deprivation or heat [9, 10].

In several cases, the potential for significant phenotypic variability has been shown to arise from the feedback structure of the regulatory network [11, 12, 13, 2]. Feedback loops are defined as molecular interactions that link the output of a system back to the input [14]. These loops ubiquitous regulatory features of biological networks and can significantly modulate the dynamics and function of circuits. For example, negative feedback can quantitatively shape cellular responses by enhancing the system's response time, reducing phenotypic variability and generating transient dynamic behaviors [15, 16, 17]. Positive feedback loops can provide signal amplification and induce bistability if the positive feedback loop is coupled to a sufficiently ultrasensitive mechanism [4, 18, 19]. Natural biological circuits frequently contain many feedback loops and it is a challenging task to disentangle the roles of individual loops and understand how their activities are coordinated in a densely connected network [13].

In this work, we have explored the role of feedback loops, dynamics and biological function of single-cell variability using the galactose gene-regulatory network (GAL) in *Saccharomyces cerevisiae* (*S. cerevisiae*) as a model system. The galactose regulatory network is a very well analyzed eukaryotic gene circuit that provides cells with the capability to metabolize the galactose as a carbon source. Extensive biochemical and molecular characterization has elucidated the key molecular events that enable cells to turn this metabolic switch on and off in response to changes in environmental signals. Here, we built upon this foundation to understand how these complex molecular interactions can combine to produce system level properties. This gene regulatory network has two interesting behaviors: single-cells can exhibit coexisting all-or-none network activity for intermediate concentrations of galactose or combinations of glucose and galactose [19, 20, 18] and small variations in concentration of galactose can generate a large fold change in the downstream enzyme levels, referred to as ultrasensitivity. Our analysis of this system identified the mechanism that generates the switch-like bistable response and revealed how this bimodal strategy can be advantageous for a population of cells in a combinatorial environment.

In Chapter 2, we use a combination of experiments and computational modeling to analyze the

roles of the feedback loops on the bimodal response of the GAL system. We demonstrate that two positive feedback loops established by the bifunctional galatokinase and signal transducer Gal1p and signal transducer Gal3p collaborate to induce bistability in the system. Our computational analysis identifies molecular sequestration as a critical mechanism for generating the ultrasensitive stage necessary for robust bistability in the system.

In Chapter 3, we probe how the GAL network integrates two signals of glucose and galactose to generate a dynamic transcriptional response. By measuring single-cell dynamics over a long time scale, we observe transient bimodality for conditions of similar concentrations of the two sugars. In fact, after many cell generations, all cells in the population converge to a single monomodal on-state. We construct a computational model that captures the structure of the network with two inputs. Our analysis of the model reveals that the observed transient bimodality originates from bistability that vanishes when glucose is depleted beyond a threshold. Sugar measurements indicate that the delayed turn-on of the repressed subpopulation of cells occurs precisely when cells begin to consume galactose following glucose depletion. The early activation of the GAL genes in a fraction of cells is shown to reduce the transition time between carbon sources and provides a transient enhancement of cellular growth rate. Our experiments also reveal a cost to constitutive GAL gene expression that arises from a reduced glucose consumption rate, thus highlighting the intricate tradeoffs involved in the timing of GAL gene induction.

In Chapter 4, we investigate the mapping between promoter sequence and expression level using the bidirectional *GAL1-10* promoter. We construct a library of randomly mutated promoter sequences and model the effects of these mutations with a statistical model to identify the relative contributions of single nucleotides to the observed expression levels. By measuring the expression levels of both directions of this bidirectional promoter, our results indicate that individual nucleotides can differentially tune the promoter activity. Experimental characterization of critical nucleotides displays a strong correlation with the model's prediction, highlighting the predictive capabilities of the model.

In Chapter 5, using a computational model of the GAL network, we analyze the roles of the feed-

back loops and sequestration on a set of phenotypes including bistability, ultrasensitivity, switching threshold, dynamic range, response time and tunability.

Chapter 2

Dual feedback loops established by molecular sequestration generates robust bimodal response

A version of this chapter has been published as [19].

Introduction

Cells are continuously faced with the challenge of sensing signals in their environment and eliciting intracellular programs accordingly. While changes in some environmental cues engender graded and proportional responses, others induce decisive action whereby a cell exhibits a binary (on or off) phenotypic change. In the latter case, amplification of phenotypic heterogeneity may arise since single cells in a population make individual decisions based on their perception of the environmental stimulus, stochastic fluctuations in their molecular components, and memory of past conditions. This thresholded cellular response can manifest as a bimodal distribution in network activity across an isogenic cell population.

Feedback regulation, which links the output of a circuit back to its input, expands the set of possible biological properties, including robustness to uncertainty [14] and can produce single cell phenotypic heterogeneity in a uniform environment. Many features of individual positive and negative feedback loops have been elucidated, including enhancement of response time and reduction of gene expression noise by negative autoregulation, and signal amplification and bistability using

positive autoregulation [15, 16, 21, 13]. However, quantitative characterization of how multiple feed-back pathways interact to regulate and fine-tune cellular decision-making presents many unresolved challenges.

The galactose gene-regulatory network *S. cerevisiae* (GAL) contains numerous feedback pathways. Isogenic single cells respond heterogeneously to a range of galactose concentrations, which manifests as a bimodal distribution of GAL gene expression across the cell population [18]. In contrast to a graded response, in which the mean of a unimodal distribution is continuously adjusted as the input is modulated, variations in the concentration of galactose within a range shifts the fraction of the cell population distributed between distinct metabolic states. Here, we focused on how the multiple feedback loops in the system shape this bimodal cellular decision-making strategy in response to galactose.

The GAL circuit consists of regulatory machinery (Gal2p, Gal3p, Gal80p, Gal4p) that dictates network activity and a set of enzymes required for metabolizing galactose (Gal1p, Gal7p, Gal10p). In the absence of galactose, GAL genes are repressed due to the sequestration of the potent transcriptional activator Gal4p by the repressor Gal80p (Fig. 2.1). [22]. In the presence of galactose, the membrane-bound permease transporter Gal2p significantly increases the rate of galactose uptake from the extracellular environment [23]. Galactose and ATP-dependent activation of the signal transducer Gal3p lead to repression of Gal80p by sequestration, thus liberating Gal4p [24]. The galactokinase Gal1p catalyzes the first step in galactose metabolism by phosphorylating galactose to form galactose 1-phosphate and has been shown to possess weak co-inducing functionality [25].

Galactose-dependent regulation of Gal2p, Gal3p and Gal80p form feedback loops because these proteins modulate network activity and are themselves transcriptionally regulated by Gal4p [27]. Gal2p and Gal3p form positive feedback loops since up-regulation of their expression levels leads to an increase in pathway activity, whereas Gal80p reduces pathway activity and thus forms a negative feedback loop.

In addition to Gal2p, Gal3p and Gal80p, there is evidence to suggest that Gal1p has a regulatory role beyond its vital enzymatic function for growth on galactose [28, 25, 29]. Gal1p is a close homolog
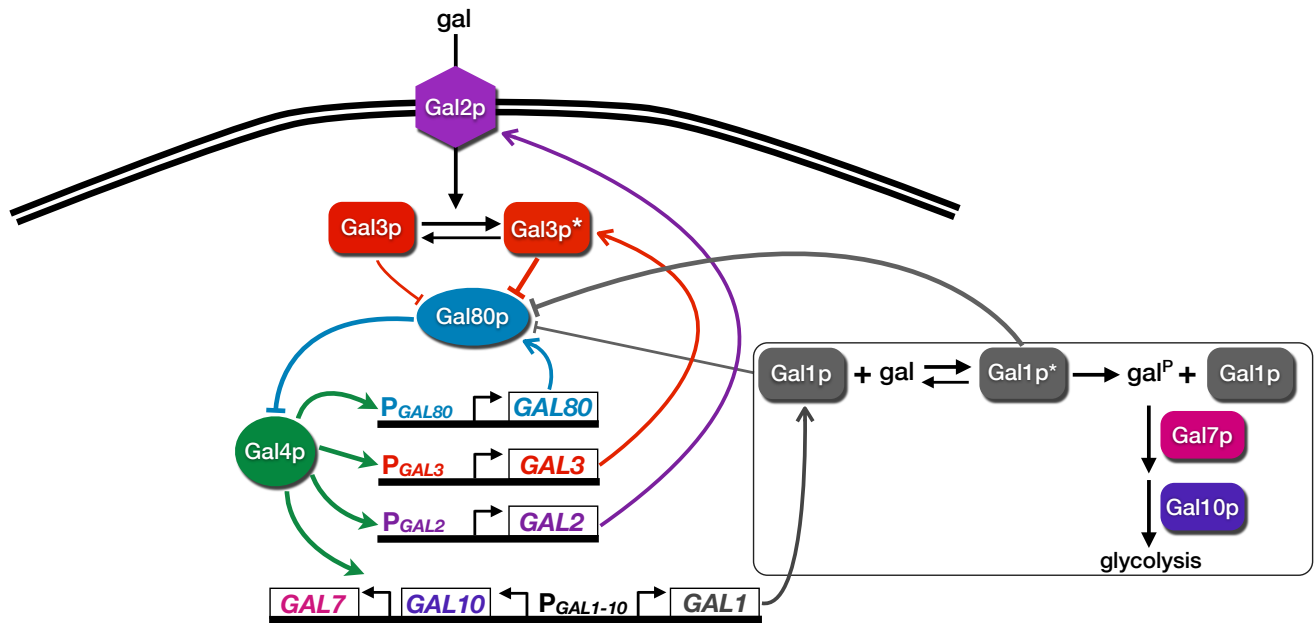
Figure 2.1: The galactose gene-regulatory network in *S. cerevisiae*. The permease Gal2p facilitates intracellular galactose transport. By binding to galactose, the signal transducer Gal3p becomes highly activated to sequester the transcriptional repressor Gal80p. In the absence of galactose, Gal3p can also inhibit Gal80p, presumably with lower affinity, leading to GAL gene induction [25]. Repression of Gal80p liberates the transcriptional activator Gal4p to up-regulate a set of target enzymatic and regulatory genes. A series of enzymatic reactions (interactions inside box) transforms galactose into glucose-6-phosphate for glycolysis through the activities of the galactokinase Gal1p, transferase Gal7p, and epimerase Gal10p. The regulatory proteins Gal2p, Gal3p and Gal80p, form positive, positive and negative feedback loops, respectively. Gal1p, a paralogue of Gal3p, has been shown to possess bifunctional activities by sequestering Gal80p in the presence and absence of galactose with different affinities, leading to GAL gene activation [25, 26]. *GAL1* and *GAL10* share a bidirectional promoter ($P_{GAL10\text{-}1}$).

of Gal3p and has been shown to interact with Gal80p with a weaker affinity than Gal3p [30, 31]. Furthermore, a *GAL3* deletion strain was shown to induce GAL gene expression at a significantly slower rate compared to wild-type whereas cells with combined *GAL1* and *GAL3* deletions fail to activate their GAL pathway [32]. A recent study demonstrated that cells initially grown in galactose and then transferred to glucose exhibit a faster induction response to a second galactose exposure than cells grown only in glucose, and that Gal1p was critical for this decrease in response time [33]. Finally, galactose induction was shown to consist of two stages, the first of which is dominated by rapid association of Gal3p to Gal80p and a delayed second stage consisting of dominance of the Gal1p-Gal80p complex [34].

In this paper, we use a combination of experimental measurements and computational modeling to demonstrate that the observed bimodality in the galactose metabolic pathway arises from an underlying bistability in the system and that this bimodal response relies on the synergistic interplay of the *GAL1* and *GAL3* feedback loops. These central mediators have unique mechanistic roles in the GAL system since they both regulate circuit activity by competitive molecular sequestration of Gal80p. While the bimodal response can be transformed into a graded response in the absence of the individual *GAL1* and *GAL3* feedback loops, this only occurs in a specific parameter regime in which the constitutive production rates of Gal1p and Gal3p are greater than a threshold. A mathematical model recapitulates the experimental results and provides crucial insights about the roles of the autoregulatory loops on bistability. More broadly, a simple mathematical model is used to identify generalizable properties of positive feedback loops created by molecular sequestration that implement robust switch-like responses.

Results

History-dependent response indicates that bimodality arises from underlying bistability and Gal1p significantly enhances sensitivity to galactose

The presence of bimodality does not necessarily imply bistability since a bimodal distribution can arise from stochastic effects [35, 36, 37]. Hysteresis is a characteristic feature of bistability, in which the system jumps from one branch of stable steady-states to a different branch of steady-states as a parameter is continuously increased, but jumps from the second branch of steady-states back to the first branch at a different value of the parameter as it is continuously decreased. This behavior stems from a difference in the local stability of multiple stable equilibria. To determine if bimodality in the GAL system was linked to bistability, we checked for a history-dependent response, which is an indicator of local equilibrium point stability. The bistable stochastic counterpart of a deterministic bistable system may not exhibit hysteresis due to an insufficient time-scale separation and a deterministic system can be bistable without displaying hysteresis [38, 39]. Here, we tested for a stochastic system that exhibits hysteresis, which would be consistent with an underlying bistability in a deterministic model of the system. Distinguishing whether bimodality arises from stochastic interactions or a deterministic bistability provides critical information about the operation of the system, including the types of molecular interactions that might be underlying this response and suggests a mathematical modeling framework for studying this phenotype.

We investigated the GAL system's history-dependent response by comparing the stability of its high and low metabolic states as a function of galactose. To measure relative expression state stability, we used flow cytometry to quantify the fluorescence distributions of a genome integrated *GAL10* promoter fusion to Venus (YFP) in wild-type (WT) single cells as an indicator of network activity [40] (P_{GAL10}Venus). The cells were grown first in the presence (E_H) and absence (E_L) of 2% galactose in 2% raffinose media. Cells from the two environments were then shifted to a second set of environments containing a wide range of galactose concentrations.

A history-dependent response existed if cell populations grown in the two environments (E_L
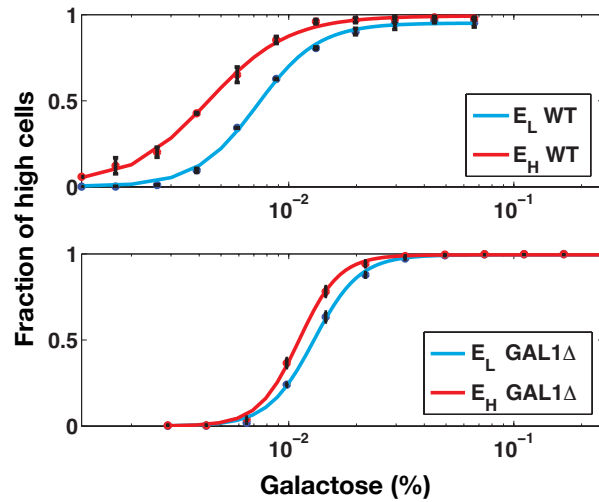
Figure 2.2: History response experiment indicates that GAL bimodal response arises from underlying bistability. **(A)** Conceptual diagram of the history response experiment in which the depth of the potential wells (expression level vs. stability) can be controlled by a bifurcation parameter (galactose concentration). In this experiment, isogenic cells were grown in two environments until steady-state, E_H and E_L. In E_H (2% galactose and 2% raffinose), the high expression state (H) has a lower potential energy and is strongly favored whereas the low expression state (L) is favored in E_L (2% raffinose). Cells are then transferred from the two initial environments to a new set of environments (E_1, ..., E_n) containing a range of galactose concentrations. A history-dependent response was present if cells from E_H and E_L were distributed differently between the high and low states for a range of galactose concentrations after 30 hours of induction. **(B)** History-dependent response experiment indicates that the GAL network is bistable. Experimental data showing history response region for wild-type (WT) cells (top) following the experimental procedure outlined in **A**. Cells that do not metabolize galactose (GAL1Δ) also displayed a history-dependent response (bottom). Each data point is the mean of the fraction of cells in the high expression state and the error bars represent one standard deviation (n=3). Lines represent fitted Hill functions.

and E_H) had a different fraction of cells distributed between the high and low expression states in a range of galactose concentrations after approximately 10 cell divisions post shift (30 hours). A 30-hour induction period was selected to allow a sufficient number of cell divisions for dilution of the fluorescent reporter from E_H cells (Section S2.1). Within a range of galactose concentrations, cells from E_L and E_H were distributed differently between the high and low metabolic states (Fig. 2.2), revealing a history-dependent response and corroborating the existence of bistability.

To exclude the possibility that the difference in the thresholds of the dose responses was due to variable consumption of galactose, the history-response experiment was performed using a *GAL1* deletion strain that is incapable of metabolizing galactose (GAL1Δ) [41]. The GAL1Δ strain was used since cells with gene deletions for the transferase *GAL7* and epimerase *GAL10* are unable to grow in the presence of galactose due to the toxic accumulation of phosphorylated galactose [42].

Investigation of history-dependence in the GAL1Δ strain revealed that its dose response threshold was approximately twofold higher than WT, demonstrating that Gal1p significantly contributes to galactose sensitivity. The GAL1Δ cells also exhibited a history-dependent difference in the galactose threshold. However, the area separating the activation response curves for GAL1Δ was smaller than WT, indicating a diminished history-dependent response. Taken together, these data corroborate bistability as the source of bimodality in the response of the GAL network to galactose and strongly suggest that Gal1p plays an important regulatory role in addition to its metabolic function.

Combined deletion of the *GAL1* and *GAL3* feedback loops produces a graded response, demonstrating the unique role of Gal1p and Gal3p in generating bistability

To further explore Gal1p as a regulatory component of the system and evaluate its role relative to the other autoregulatory loops, we constructed a series of feedback loop deletions involving different components of the system. To do so, we deleted the coding region of a given gene and integrated a single copy of this gene regulated by an inducible *TET* promoter or a constitutive promoter. The rate of production from the *TET* promoter could be adjusted by a doxycycline (dox) dependent

activation of rtTA, a reverse mutant of the transcription factor, TetR [43]. In this fashion, the expression of the gene involved in the feedback loop can be decoupled from the activity of the galactose pathway since the regulation of the constitutive or inducible promoter is external to the GAL regulatory circuit.

In order to compare the operation of the WT system and the different feedback mutants on equal footing, we selected the strength of constitutive expression of each gene by mapping it to the corresponding WT expression levels using quantitative real-time PCR (qPCR) (Table 1 and Supplementary Fig. 2.3). We also explored a range of *TET* promoter expression levels by scanning different dox concentrations to investigate the relationship between constitutive expression of each regulatory component and the steady-state dose response. The fluorescence distributions were classified as unimodal or bimodal using a Gaussian mixture model threshold (GMM) (see Materials and methods).

Eliminating the *GAL2* or *GAL80* feedback loops did not abolish the GAL system's bimodal response (Fig. 3B-1 and B-2). Instead, bimodality persisted for a range of expression levels for Gal2p and Gal80p (Supplementary Fig. 2.5B,C). Compared to WT, cells with a deleted *GAL80* feedback loop (*GAL80Δ* fb) displayed bimodality for a larger number of galactose concentrations. Contrary to a previous study [20], we observed that the *GAL3* feedback loop was not necessary for bimodality for WT expression levels of Gal3p (Fig. 3A-4 and Supplementary Fig. 2.2). However in the GAL3Δ fb cells, the bimodal response could be transformed into a graded response by driving the rate of constitutive Gal3p production beyond a critical threshold (Fig. 5B). We found that the discrepancy with the previous study [20] can be explained by constitutive Gal3p expression above this threshold (Section S2.2).

Since the *GAL2*, *GAL3* and *GAL80* feedback loops were not individually necessary for bimodality, we hypothesized that they either play compensatory roles or that bimodality relies on yet another uncharacterized feedback loop. To address the possibility that the feedback loops had overlapping or compensatory functions, we constructed combinations of feedback loop deletions of *GAL2*, *GAL3* and *GAL80* by constitutively expressing them from the *ADH1*, *TET* and *STE5* promoters, respec-
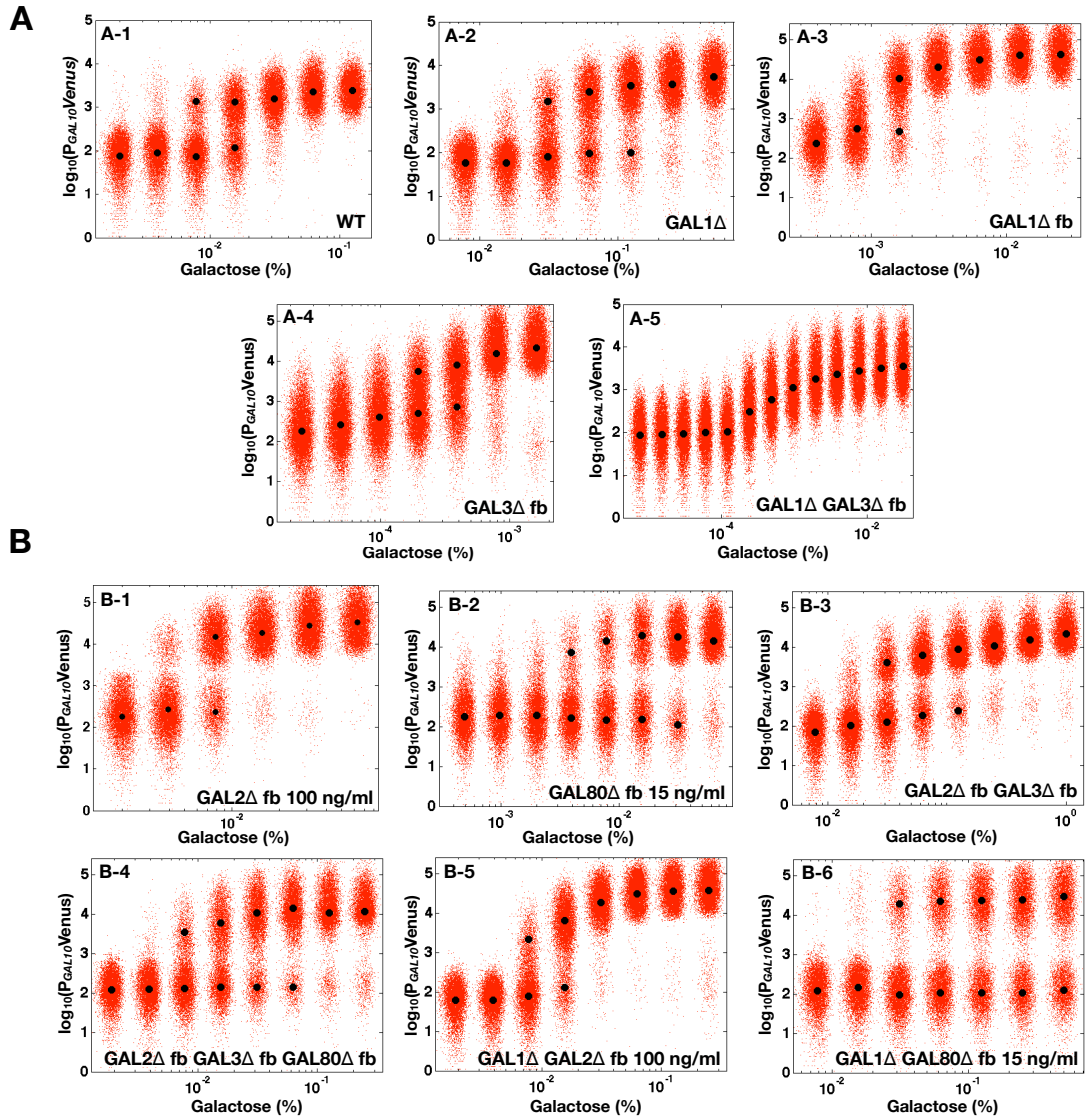
Figure 2.3: Double deletion of *GAL1* and the *GAL3* feedback loop abolishes bimodality. Representative steady-state flow cytometry data of P_{GAL10}Venus in wild-type (WT) and a set of single and multiple feedback loop deletions induced with a range of galactose concentrations. Each black circle indicates the mean of the distribution determined by a Gaussian mixture model (see Materials and methods). Small random deviations were added to each galactose concentration to highlight the spread of the fluorescence distributions. **(A)** Either the *GAL1* or the *GAL3* feedback loop is required for bimodality. The wild-type (WT), *GAL1* deletion (GAL1Δ), *GAL1* feedback deletion (GAL1Δ fb) and *GAL3* feedback deletion (GAL3Δ fb) strains displayed bimodality for at least one galactose concentration. GAL1Δ fb and GAL3Δ fb were not induced with doxycycline (dox). Eliminating the *GAL3* feedback loop in the absence of *GAL1* (GAL1Δ GAL3Δ fb) produced a graded response for the full range of galactose. **(B)** Bimodality was preserved for a series of feedback loop disruptions. The single *GAL2* (GAL2Δ fb) and *GAL80* (GAL80Δ fb) loop deletions were induced with 100 and 15 ng/ml dox, respectively. Bimodality persisted for a dual feedback loop disruption of *GAL2* and *GAL3* (GAL1Δ fb GAL3Δ fb) and a triple feedback deletion of *GAL2*, *GAL3* and *GAL80* (GAL2Δ fb GAL3Δ fb GAL80Δ fb). For these two strains, *GAL2*, *GAL3* and *GAL80* were expressed from an *ADH1*, *TET* and *STE5* promoter, respectively in the absence of dox. Deleting the *GAL2* (GAL1Δ GAL2Δ fb) and *GAL80* (GAL1Δ GAL80Δ fb) feedback loops individually in a strain lacking *GAL1* preserved bimodality. GAL1Δ GAL2Δ fb and GAL1Δ GAL80Δ fb were induced with 100 and 15 ng/ml dox, respectively.

tively. Remarkably, bimodality was preserved in the absence of both the *GAL2* and *GAL3* feedback loops (GAL2Δ fb GAL3Δ fb) and also in a triple feedback loop deletion strain of *GAL2*, *GAL3* and *GAL80* (Fig. 3B-3 and B-4).

Therefore, combinations of *GAL2*, *GAL3* and *GAL80* feedback loops did not functionally overlap to create bimodality. Since Gal1p regulates both sensitivity and memory of the GAL network to galactose (Fig. 2.2), we explored the possibility that Gal1p could be an important component of the system's bimodality.

In contrast to Gal3p and Gal80p transcriptional regulation, Gal1p is tightly repressed in the absence and strongly induced in the presence of galactose. As a consequence, matching the open and closed loop production rates using the *TET* promoter was challenging. Similar to Gal3p, Gal1p has been shown to activate GAL genes independently of galactose, and a sufficiently strong constitutive Gal1p production rate could shift the operating point of the network [25]. We first explored the lowest regime of Gal1p expression using a *GAL1* gene deletion (GAL1Δ) and bimodality was detected in this strain for several galactose concentrations (Fig. 2.3A-2). The *GAL1* feedback loop deletion, P$_{TET}$GAL1 (GAL1Δ fb) was also bimodal in the absence of dox for at least one galactose concentration (Fig. 2.3A-3) but was graded in the presence of 10, 25, 50 and 100 ng/ml doxycycline (Supplementary Fig. 2.4).

We examined the combined effect of removing the *GAL2*, *GAL3* or *GAL80* in a strain lacking *GAL1*. As shown in Fig. 2.3B-5, B-6, the combined deletion of *GAL1* and the *GAL2* feedback loop (GAL1Δ GAL2Δ fb) and dual deletion of *GAL1* and the *GAL80* feedback loop (GAL1Δ GAL80Δ fb) displayed bimodality for at least two galactose concentrations.

By stark contrast, the simultaneous deletion of *GAL1* and the *GAL3* feedback loop (GAL1Δ GAL3Δ fb) produced a graded response for the entire range of galactose (Fig. 2.3A-5). Remarkably, this graded response persisted irrespective of the constitutive Gal3p production rate in contrast to the single *GAL3* feedback knockout that displayed bimodality for some range of constitutive Gal3p levels (Supplementary Fig. 2.5A). These data provide further evidence that *GAL1* is an active regulatory component of the circuit and that the interplay between the *GAL1* and *GAL3* feedback

loops is crucial for bimodality.

In addition to eliminating bimodality, our results revealed that removing $GAL1$ and the $GAL3$ feedback loop abolished ultrasensitivity in the dose-response to galactose, indicating a coupling between the mechanisms for ultrasensitivity and bistability in the GAL network. We found that the Hill coefficient for P_{GAL10} Venus in WT was approximately 3 whereas this same reporter exhibited a Hill coefficient of approximately 1.3 in the absence of $GAL1$ and the $GAL3$ feedback loop (GAL1Δ GAL3Δ fb) (Supplementary Fig. 2.5D). This link between ultrasensitivity and bimodality may arise due to the necessity of ultrasensitivity for bistability [44].

Cooperative Gal4p interactions at the promoter level does not generate bimodal response

Bimodality was not observed using the $GAL3$ and $GAL80$ promoters as reporters of GAL network activity in WT for any concentration of galactose (Supplementary Fig. 2.1C). In contrast to the $GAL10$ promoter, these promoters each contain a single $GAL4$ binding site. Multiple $GAL4$ binding sites may augment the dynamic range of the reporter to provide a sufficient separation of the high and low expression states or cooperativity of Gal4 proteins at the promoter level may be an important parameter of the bimodal response. To test whether multiple $GAL4$ binding sites are necessary for bimodality, a synthetic GAL promoter containing a single Gal4p binding site from the $GAL7$ promoter driving the expression of a fluorescent reporter was constructed (see Materials and methods). This reporter had minimal cooperativity and yet bimodality was detected for two galactose concentrations at steady-state (Supplementary Fig. 2.6). These data demonstrate that bimodality is not an exclusive property of promoters with multiple $GAL4$ binding sites but is instead a property of the upstream regulatory network.

Deterministic model of GAL network recapitulates experimental results and provides insights into the roles of feedback loops

To further probe the roles of the feedback loops, we constructed an ordinary differential equation (ODE) model of the system (Section S2.4) which takes into account the concentrations of Gal1p (G1), Gal3p (G3), Gal4p (G4) and Gal80p (G80). Since Gal1p and Gal3p can function as co-inducers of GAL gene expression independently of galactose, presumably with lower affinities than the galactose bound forms, these different forms were not differentiated in the model [25].

Based on these assumptions (see Section S2.4 for a full description), the set of differential equations for G1, G3, G4 and G80 that model the interactions shown in Fig. 2.1 is given by

$$\frac{d[\text{G1}]}{dt} = \alpha_{gal}\epsilon + \frac{\alpha_{G1}[\text{G4}]^3}{[\text{G4}]^3 + K_{G1}^3} + \omega[\text{G1}][\text{G80}] - \gamma_{G1}[\text{G1}],$$

$$\frac{d[\text{G3}]}{dt} = \alpha_{gal} + \frac{\alpha_{G3}[\text{G4}]^2}{[\text{G4}]^2 + K_{G3}^2} + \delta[\text{G3}][\text{G80}] - \gamma_{G3}[\text{G3}],$$

$$\frac{d[\text{G4}]}{dt} = \alpha_{G4} + \beta[\text{G80}][\text{G4}] - \gamma_{G4}[\text{G4}],$$

$$\frac{d[\text{G80}]}{dt} = \alpha_{oG80} + \frac{\alpha_{G80}[\text{G4}]^2}{[\text{G4}^2 + K_{G80}^2} + \omega[\text{G1}][\text{G80}] + \delta[\text{G3}][\text{G80}] + \beta[\text{G80}][\text{G4}] - \gamma_{G80}[\text{G80}].$$

Here, α_{gal} represents galactose as a constant input rate. Parameters were approximated from experimental measurements and values from the literature (Section S2.5). Using these estimates, the Hill coefficients for the feedback functions involving *GAL1*, *GAL3* and *GAL80* were set to 3, 2 and 2, respectively, but our conclusions were not sensitive to variations in these values. Models of the individual *GAL1*, *GAL3*, *GAL80* and combined *GAL1* and *GAL3* feedback knockouts (GAL1Δ fb, GAL3Δ fb, GAL80Δ fb, GAL1Δ GAL3Δ fb, respectively) were constructed by modifying appropriate terms in the WT model (Section S2.6).

Bifurcation analysis of GAL model confirms that only the combined *GAL1* and *GAL3* feedback deletion eliminates bistability

At equilibrium, the concentration of Gal4p can be written as an eleventh-order polynomial as described in Section S2.4. Similarly, the individual feedback deletion models for *GAL1*, *GAL3* and

GAL80 and combined *GAL1*, *GAL3* were simplified to an eighth, ninth, ninth and sixth order polynomials, respectively (Section S2.6). The roots of these polynomials include the equilibrium concentrations of Gal4p, which represents the activity of the GAL network. All of the models had the potential for bistability for some region of parameter space since the degrees of the polynomials were larger than a quadratic. Indeed, models with individual feedback deletions were still capable of bistability as a function of α_{gal} (Fig. 2.4A-1, A-2, A-3 and A-4). By contrast, removing both the *GAL1* and *GAL3* feedback loops abolished bistability for the entire range of α_{gal}, consistent with experimental data (Fig. 2.4A-5 and A-6).

GAL1 and *GAL3* feedback loops combine synergistically to augment bistability

Using the model, we explored the effects of the *GAL1* and *GAL3* feedback loops on the range of α_{gal} for which the system exhibits bistability. We defined the hysteresis strength D_H as the difference between the bifurcation points of α_{gal} as shown in Fig. 2.4A-1 (see Materials and methods). D_H represents the range of conditions in which the system exhibits bistability and thus the robustness of bistability to parameter variations increases with D_H. The *GAL1* and *GAL3* feedback deletion models had approximately 48% and 31% D_H compared to WT (Fig. 2.4B). By contrast, removing the *GAL80* feedback significantly increased D_H to 166% compared to its WT value, indicating that this negative autoregulatory loop undermines bistability.

The generality of these results and the dependence on parameters were explored by comparing the D_H of the WT and feedback deletions using randomly generated parameter sets. 10,000 parameter sets were obtained by sampling a normal distribution with mean equal to the values of parameter set I and coefficient of variation equal to 0.1. All parameters were varied except for the constitutive production rates of Gal1p (α_{G1s}), Gal3p (α_{G3s}) and Gal80p (α_{G80s}). This computation confirmed that GAL80Δ fb had a larger D_H compared to WT and that the WT exhibited a larger D_H than either of the GAL1Δ fb or GAL3Δ fb models for all parameter sets (Fig. 2.4C). These findings are consistent with the experimental characterization of history-dependent response of the GAL1Δ strain (Fig. 2.2B) and the data showing that range of galactose concentrations that produced bimodality
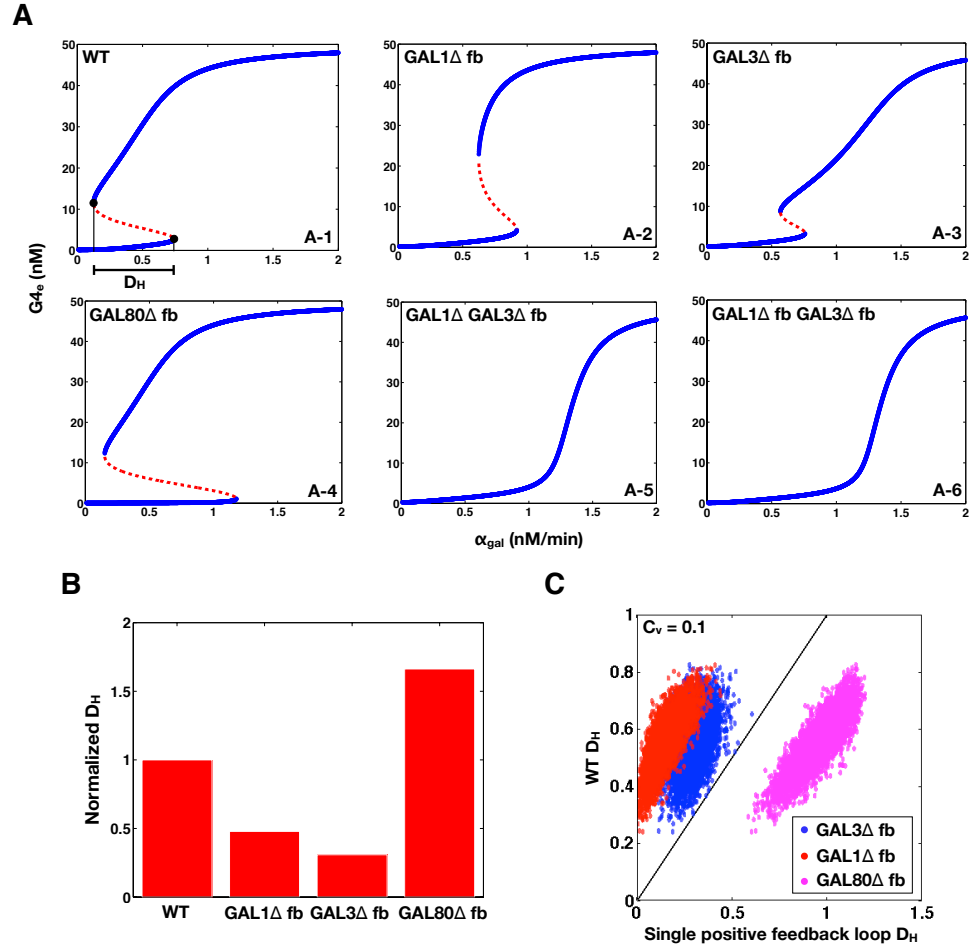
Figure 2.4: Bifurcation analysis of GAL model qualitatively matches experimental results and reveals that the *GAL1* and *GAL3* feedback loops combine synergistically to expand the parameter region for bistability. The bifurcation parameter α_{gal} represents galactose and the equilibrium value of Gal4p ($G4_e$) represents the activity level of the GAL network. **(A)** Bifurcation plots of wild-type (WT) and the feedback deletions of *GAL1* (GAL1Δ fb), *GAL3* (GAL3Δ fb), *GAL80* (GAL80Δ fb) and combined *GAL1* and *GAL3* (GAL1Δ GAL3Δ fb and GAL1Δ fb GAL3Δ fb). Blue and red represent stable and unstable equilibrium points, respectively. Reflecting the experimental results in Fig. 3, WT, GAL3Δ fb, GAL1Δ fb and GAL80Δ fb exhibits bistability whereas GAL1Δ GAL3Δ fb and GAL1Δ fb GAL3Δ fb are monostable for the full range of α_{gal}. A representative distance between the bifurcation points, D_H, is highlighted by a solid black line. **(B)** Quantification of the range of bistability for the WT and single feedback knockouts shown in **A**. Normalized D_H is equal to the range of α_{gal} that produces bistability relative to WT. **(C)** Comparison of D_H in the WT, GAL1Δ fb (blue), GAL3Δ fb (red) and GAL80Δ fb (magenta) models for 5000 representative randomly generated parameters sets sampled from a normal distribution with $C_v = 0.1$. Data points above the $x = y$ line (black) correspond to parameter sets where D_H is larger in WT compared to the single feedback loop knockouts.

was expanded in the absence of the *GAL80* feedback loop (Fig. 2.3B-2).

In summary, collaboration between the *GAL1* and *GAL3* autoregulatory loops expands the region of bistability across a broad region of parameter space, suggesting that this synergy between dual positive feedback loops may be a consequence of the unique regulatory roles of Gal1p and Gal3p in the GAL circuit. In addition, we found that GAL1Δ fb GAL3Δfb and GAL1Δ fb GAL3Δfb were monostable for all 10,000 parameter sets, indicating that one of these autoregulatory loops is necessary for generating bistability across a broad region of parameter space.

Recently, a two-stage galactose induction model has been proposed whereby the Gal3p-Gal80p complex (C83) dominates initially and the Gal1p-Gal80 complex (C81) dominates at a later stage [34]. To check the consequences of including this feature in our model, we scanned over a wide range of parameters using the Latin hypercube sampling method [45] (Section S2.5) and identified sets of parameters that qualitatively matched all of our data in addition to the dynamic ordering response of C83 and C81 (Supplementary Fig. 2.7B,C). This new parameter set exhibited the same roles for the *GAL1* and *GAL3* feedback loops in enhancing D$_\text{H}$ across a broad region of parameter space, further illustrating the generality of our results (Supplementary Fig. 2.7D).

Constitutive production of Gal1p and Gal3p can abolish bimodality in the absence of the individual *GAL1* and *GAL3* feedback loops

We next tested whether the model could predict and explain the disappearance of bimodality due to high unregulated levels of Gal1p and Gal3p in the absence of their individual feedback loops (Fig. 2.5, Supplementary Fig. 2.2 and Supplementary Fig. 2.4). The individual *GAL1* and *GAL3* feedback loop deletion models predicted the loss of bistability as the rates of constitutive production, α_{G1s} or α_{G3s}, was increased (Fig. 2.5C,D). An increase in α_{G1s} in the GAL1Δ fb model caused the bistable region to contract and vanish at a critical value ($\alpha_{G1s} = 4$) (Fig. 2.5C). In the GAL3Δ fb model, increasing α_{G3s} caused the bistable region to shift to smaller values of α_{gal} (Fig. 2.5D) and eventually move out the positive orthant to negative values of α_{gal} at a critical α_{G3s} ($\alpha_{G3s} = 1$), thus producing monostability for all physically realistic values of α_{gal}.
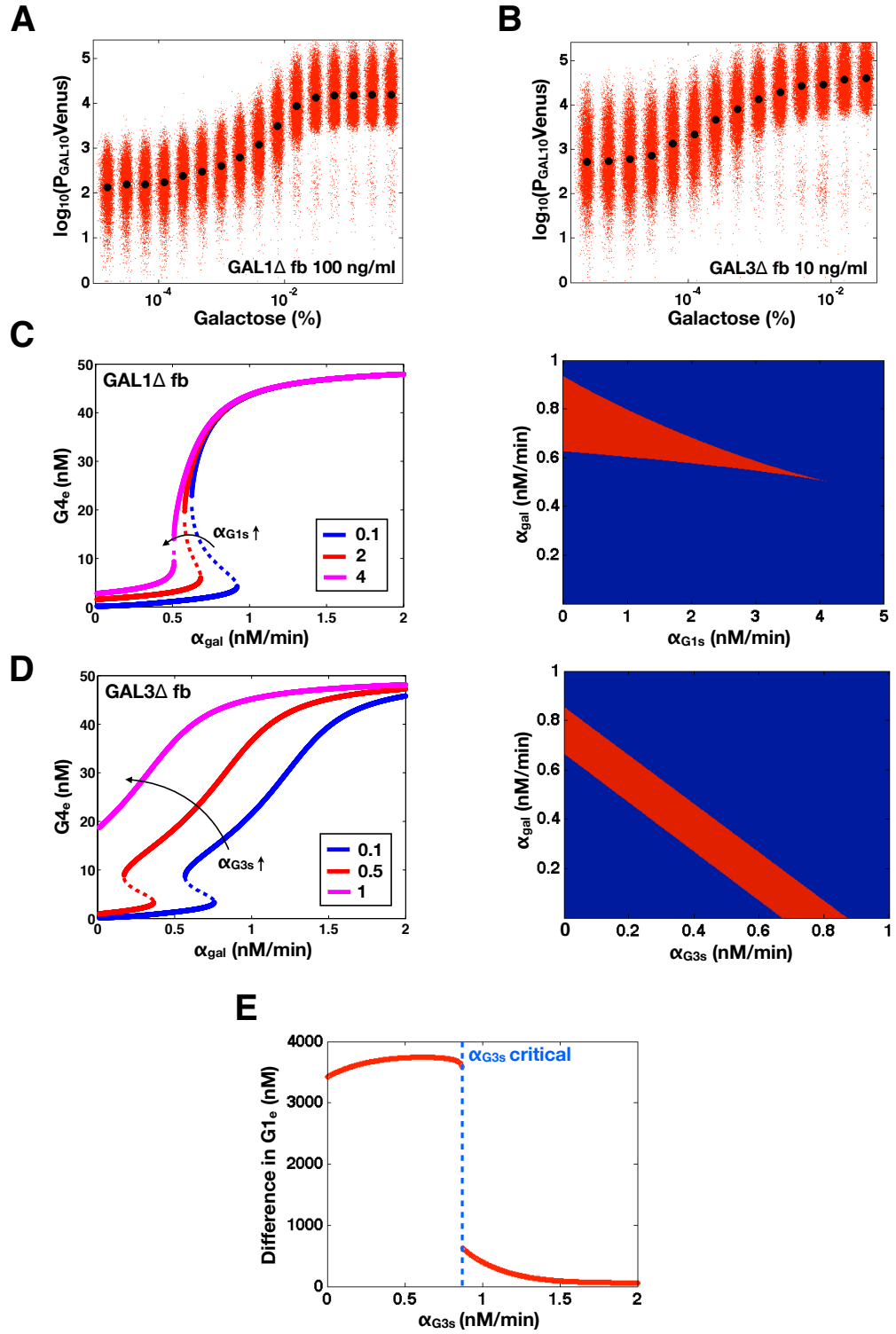
Figure 2.5

Figure 2.5: Model predicts that constitutive production of Gal1p or Gal3p above a threshold can abolish bistability in the absence of the individual *GAL1* or *GAL3* feedback loops (matching experimental data in Section S2.2, Supplementary Fig. 2.2 and Supplementary Fig. 2.4). **(A)** Critical constitutive level of Gal1p in the absence of the *GAL1* feedback loop produced a graded response. Flow cytometry measurements of P$_{GAL10}$Venus in a *GAL1* feedback deletion strain (GAL1Δ fb). In this strain, *GAL1* was expressed from a *TET* promoter and induced with 100 ng/ml doxycycline (dox), corresponding to approximately 20% of fully induced wild-type (WT) levels (Supplementary Fig. 2.3A-1). **(B)** Critical level of Gal3p in the absence of the *GAL3* feedback loop produced a graded response. Flow cytometry measurements of the *GAL3* feedback deletion strain (GAL3Δ fb). *GAL3* was expressed from a *TET* promoter and induced with 10 ng/ml dox, corresponding to approximately 63% of fully induced WT levels (Supplementary Fig. 2.3A-3). **(C)** In the GAL1Δ fb model, increasing the constitutive production rate of Gal1p (α_{G1s}) decreases the region of bistability and causes bistability to vanish at a critical value ($\alpha_{G1s} = 4$ nM/min). Regions of bistability (red) and monostability (blue) for different values of α_{G1s} and α_{gal} in GAL1Δ fb shows that the bistability parameter region contracts and eventually vanishes with increasing α_{G1s}. **(D)** In the GAL3Δ fb model, increasing the constitutive production rate of Gal3p (α_{G3s}) eliminates bistability by shifting the bistable region to smaller α_{gal} values. A critical threshold of α_{G3s} ($\alpha_{G3s} = 1$ nM/min) causes the bistable region to move out of the positive orthant, producing monostability for all physically realistic α_{gal} values. Regions of bistability (red) and monostability (blue) for different values of α_{G3s} and α_{gal}. **(E)** The *GAL1* feedback nonlinearity disappears with increasing α_{G3s} in the GAL3Δ fb model. The maximum difference in Gal1p steady-state concentration (G1$_e$) was computed across the full range of α_{gal} for a series of α_{G3s} values and represents the activity of the *GAL1* feedback loop. Above the critical α_{G3s} threshold (dashed blue line), G1$_e$ does not change in response α_{gal}, indicating that the *GAL1* autoregulatory loop is not active in this parameter regime.

Since Gal1p and Gal3p played an important role in generating bistability, we suspected that the disappearance of bistable behavior for α_{G3s} or α_{G1s} exceeding critical values could be the result of an indirect neutralization of the remaining loop. For example, it could be case that overexpression of Gal3p in a *GAL3* feedback deletion had the effect of neutralizing the *GAL1* feedback loop. The computational model afforded us the possibility of testing this hypothesis. For a given value of α_{G3s}, we defined the *GAL1* feedback activity as the maximum change in steady-state Gal1p concentration (G1$_e$) across the full range of galactose ($\alpha_{gal} = 0 - 2$ nM/min). As shown in Fig. 2.5E, the *GAL1* feedback was highly active for a range of α_{G3s} values but abruptly approached zero at a critical threshold of α_{G3s} (dashed blue line). Therefore, increasing the constitutive production rate of Gal3p was indeed equivalent to removing the *GAL1* feedback since a sufficiently large α_{G3s} mapped the *GAL1* feedback nonlinearity to a saturated (inactive) regime.

The insight generated by the model about the link between the constitutive production rates of Gal1p or Gal3p and the loss of bistability suggested that the graded response observed in GAL3Δ fb (Fig. 2.5B) should be the result of overexpressing the Gal3 protein. To test this possibility, we

compared the *GAL3* mRNA expressed from the *TET* promoter to that of WT induced with 0.005% and 0.05% galactose using qPCR. These data showed that the *GAL3* mRNA level in GAL3Δ fb induced with 10 ng/ml dox was overexpressed by 43% relative to WT induced with 0.05% galactose, significantly higher than *GAL3* mRNA levels for the bimodal range of WT and GAL3Δ fb (Supplementary Fig. 2.3A-3). These results argue that in order to study the functional contribution of feedback loops to a phenotype, the strength of constitutive expression needs to be carefully tuned in order to recapitulate the physiological operating point(s) of the wild-type circuit.

Properties of positive feedback loops established by molecular sequestration

Sequestration binding affinity of an activator and repressor can tune the range of conditions for bistability

To generalize our results further, we explored the principles by which the interactions of the positive feedback loops mediated by Gal1p and Gal3p generate bistability. Characterizing the set of essential molecular interactions that combine to generate bistability in the GAL system may be useful for analyzing other natural switch-like biological networks and for constructing robust and tunable bistable synthetic circuits. Gal1p and Gal3p competitively sequester a common protein, Gal80p. Competitive binding interactions and molecular sequestration can produce ultrasensitivity, which is crucial building block for a bistable system [46, 47, 48, 49]. Therefore, we suspected that the competitive sequestration of Gal80p by Gal1p and Gal3p may constitute a critical feature of the system.

To probe the functionalities provided by positive feedback loops linked to molecular sequestration, we examined a simple model of a single positive feedback loop that is implemented by an activator x that can form an inactive complex with a transcriptional repressor z. In this circuit, z transcriptionally represses the production of x and therefore a positive feedback loop is established by inhibition of the transcriptional repressor using molecular sequestration (Supplementary Fig. 2.8A). We first examined the parameter dependence of this system in the absence of transcriptional

cooperativity and found that this circuit could exhibit bistability depending on the value of the binding affinity of the activator and repressor (Supplementary Fig. 2.8B). Therefore, modifying this parameter is an alternative mechanism to induce bistability in the circuit without increasing the cooperativity.

Building on these results, we next investigated the roles of double positive feedback loops connected by molecular sequestration. We considered a three-state ODE model consisting of a transcriptional repressor z that directly regulates two activators, x_1 and x_2 with Hill coefficients of 3 and 2, respectively. x_1 and x_2 can form inactive heterodimers with z and hence x_1 and x_2 compete to bind z (Fig. 2.6A). In this model, the mechanisms of sequestration and positive feedback are triggered by an input (u) that represents a basal production rate of x_1 and x_2. The system of equations that model the interactions in Fig. 2.6A (see Section S2.7 for a full description) is

$$\frac{dx_1}{dt} = u + \frac{\alpha_1 K_1^3}{K_1^3 + z^3} + \beta_1 x_1 z - \gamma_1 x_1,$$

$$\frac{dx_2}{dt} = u + \frac{\alpha_2 K_2^2}{K_2^2 + z^2} + \beta_2 x_2 z - \gamma_2 x_2,$$

$$\frac{dz}{dt} = \alpha_z + \beta_1 x_1 z + \beta_2 x_2 z - \gamma_z z.$$

In the double positive feedback case, bistability could be induced in this system by adjusting the binding affinities K_{D1} and K_{D2} (which modify β_1 and β_2) as bifurcation parameters without changing the cooperativity of the transcriptional regulation (Fig. 2.6B,C). Setting $K_{D1} = K_{D2}$, we found that the range of the input that produced bistability was inversely related to the magnitude of the binding affinities (Fig. 2.6B). In addition, the range of the input that generated bistability was increased in a system with two positive feedback loops compared to a single positive feedback loop for the set of symmetrically varying K_{D1} and K_{D2} values (Fig. 2.6C).

To explore asymmetry in the binding affinities, D_H was computed for a series of linearly spaced K_{D1} and K_{D2} values within the range of 0.5-80 nM (Fig. 2.6D). The largest range of bistability was obtained for the strongest binding affinities and D_H decreased monotonically with increasing K_{D1} or K_{D2}. In addition, fixing one K_D while varying the other (left column and bottom row)
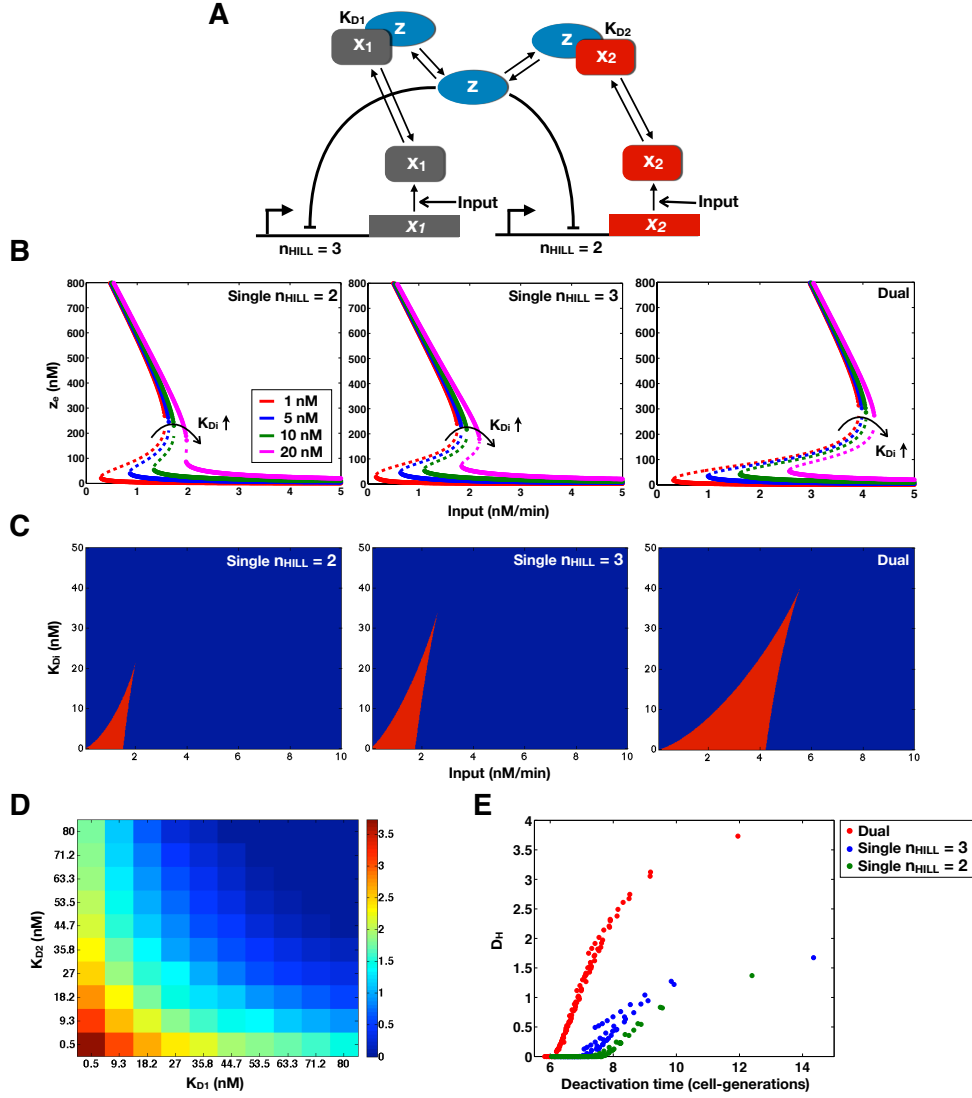
Figure 2.6: Molecular consequences of positive feedback loops established by molecular sequestration. Sequestration binding affinities (K_{D1} and K_{D2}) can tune the parameter region for bistability and the addition of a second positive feedback loop can reduce the deactivation response time and augment the range of conditions for bistability. **(A)** Circuit diagram for dual positive feedback loops mediated by the activators, x_1 and x_2 coupled by molecular sequestration to a transcriptional repressor (z). Transcriptional feedback regulation of x_1 and x_2 are modeled by Hill functions with Hill coefficients of 3 and 2. The single positive feedback loop models were obtained by removing the appropriate repression arrow from z to the promoter of x_1 or x_2 or equivalently, replacing the Hill functions with a constant production rate, α_{1s} or α_{2s}. **(B)** Bifurcation diagrams relating the input to the steady-state concentration of z (z_e) reveal that symmetrically weakening the binding affinities shrinks the region of bistability. **(C)** Parameter regions of bistability (red) and monostability (blue) for different values of the input and symmetrically varying K_{D1}, K_{D2} in the single and double feedback loop models. **(D)** Range of bistability (D_H) for a range of K_{D1} and K_{D2} values in the double feedback loop system. **(E)** Relationship between D_H and the deactivation response time measured in cell-generations (see Section S2.7). For a constant nonzero D_H, the dual feedback loop circuit exhibited a faster deactivation response time compared to the either of the single positive feedback loop models.

did not decrease D_H as significantly as symmetrically changing the two binding affinities together (diagonal). These results suggest that asymmetry in the binding affinity strengths whereby one activator interacts strongly and the other activator binds weakly to the same repressor can preserve bistability over a wide range of values for the weaker K_D, thus reducing the system's sensitivity to variations in this parameter.

Double positive feedback loops can produce larger range of bistability and a faster dynamic response than a single feedback loop

We suspected that modulating the binding affinities to induce bistability may concurrently alter other circuit functions such as the dynamic response time to a change in the input. To explore these relationships, we measured the response times of the circuits to switch from the low→high state (activation response time) and from the high→low state (deactivation response time). To do so, a step function increase or decrease in the input was applied and the delay for the circuit to adapt to this transition was quantified (see Section S2.7). The time required for an output species that was transcriptionally repressed by z (representing a fluorescent reporter) to increase or decay to half its maximum value was quantified in cell-generations.

In the double feedback loop system, the activation response time decreased with the strength of the binding affinities whereas the deactivation response time had the opposing relationship and increased with the strength of this binding affinities (Supplementary Fig. 2.8C,D). For a constant nonzero D_H, the dual feedback loop system could switch faster to the high state than either of the single feedback loop models (Supplementary Fig. 2.8E). Since both the D_H and the deactivation response time are inversely related to K_{D1} and K_{D2}, a tradeoff exists between increasing the range of conditions for bistability and decreasing the deactivation response time (Fig. 2.6E). A comparison of D_H and the response times for the single and double feedback loop systems revealed that dual feedback loops can produce a larger D_H over a narrower range of deactivation response times compared to the single feedback loop systems with Hill coefficients of 2 or 3. Taken together, the dual feedback loop system can produce a larger range of bistability and exhibit a faster response

time to abrupt changes in the environment compared to a single feedback loop system.

Discussion

A bimodal distribution of gene expression across a population of isogenic cells, which generates two distinct cellular states, can produce significant cell-to-cell heterogeneity. This bimodality can also lead to a switch-like response that filters out noise below a threshold and produces a large fold-change in the system's output if the input crosses this threshold [50]. In this work, we used the GAL gene-regulatory circuit as a model system to dissect and analyze the origins of bimodality in a natural biological network. We demonstrated that bistability underlies this bimodality and used a combination of experiments and computational modeling to identify two key features that produce bistability: (1) a threshold established by two positive feedback loops mediated by Gal1p and Gal3p and (2) an ultrasensitive stage produced by competitive molecular sequestration of Gal80p by Gal1p and Gal3p.

To unravel the molecular interactions critical for bistability in the GAL system, we performed a comprehensive exploration of multiple feedback loops. Our investigations revealed that the GAL bimodal response is remarkably robust to feedback loop perturbations. Indeed, individual elimination of the *GAL1*, *GAL2*, *GAL3*, and *GAL80* feedback loops was insufficient to abolish bimodality. Furthermore, bimodality persisted for multiple deletions of these loops and, surprisingly, only disappeared in a double deletion of *GAL1* and the *GAL3* feedback loop. We therefore identified Gal1p and Gal3p as central mediators of two synergistic positive feedback loops that generate bistability in the GAL gene-regulatory network. Multiple positive feedback loops can facilitate the bistable behavior of a circuit by expanding the range of conditions for bistability, which improves the robustness of bistability to parameter variations [50].

A previous study attributed bimodality in the GAL pathway to the activity of the *GAL3* feedback loop [20]. Here we demonstrate that cells with a deleted *GAL3* feedback loop are still capable of bimodality in their response to galactose for low levels of constitutive Gal3p expression. However, we found experimentally that bimodality vanishes when Gal3p is expressed at high and unregulated

levels. Our computational model explains this behavior by the loss of remaining *GAL1* feedback due to constitutive expression of Gal3p beyond a threshold. Interestingly, in this regime, the genetic wiring of the *GAL1* feedback loop is present, but the feedback loop was rendered inactive indirectly by constitutive Gal3p expression above a threshold.

These results underscore the challenges inherent in the interpretation of feedback deletion experiments in which the specific range of constitutive expression of the deleted link might become an important determinant of the system's properties and can mask the true functional roles of the feedback pathway. These findings also argue that the complete interpretation of feedback knockouts requires thorough investigation of active mechanisms and nonlinearities that are operational in a given circuit, beyond static snapshots of the circuit's topology as determined by genetics [51].

Stoichiometric binding interactions, for example, molecular sequestration of a repressor by an activator or inhibition of an enzyme by a small molecule, can produce ultrasensitivity in biological circuits [46, 47, 48, 49, 52]. Our computational model indicates that competitive molecular sequestration of Gal80p by Gal1p and Gal3p produces an ultrasensitive change in the concentration of free Gal4p in response to a small variations in extracellular galactose and this ultrasensitivity does not rely on cooperative binding of Gal4p to GAL promoters and/or oligomerization. These results suggest that the stoichiometric inhibition of Gal80p by Gal1p and Gal3p is a crucial source of ultrasensitivity in the GAL network that sets the stage for a robust bistable response to galactose since ultrasensitivity is required for bistability [53, 49].

Beyond the GAL system, we believe these results to be applicable to many bistable systems. We used a simple computational model to explore the general mechanisms by which positive feedback loops linked to competitive sequestration can produce ultrasensitivity and bistability. Using this model, we found that the positive feedback and sequestration topology can be used to build a bistable system in the absence of transcriptional cooperativity by adjusting the binding affinity parameter between the activator and inhibitor. If bistability confers an fitness advantage, this parameter could be adjusted through mutation of the protein-protein binding interface and may be more evolvable than modifying the cooperativity of transcriptional regulation through oligomerization or multiple

transcription factor binding sites. In addition, we identified a tradeoff between the range of bistability and the deactivation response time of this circuit. In response to an abrupt change in the stimulus, we found that a system with double positive feedback loops can switch faster to the low state compared to the single feedback loop system for a fixed range of bistability, highlighting a novel advantage of multiple positive feedback loops.

Positive feedback loops established by molecular sequestration may represent a general class of systems for implementing robust switch-like cellular responses. For example, the conserved regulatory network that controls cell-differentiation in *Drosophila* consists of similar molecular mechanisms to the GAL circuit including molecular sequestration and multiple feedback loops that implement a switch-like developmental program [54, 55]. Activation of this cell-differentiation circuit relies on molecular titration of a repressor, Extramacrochaetae (Emc) by the activators Daughterless (Da) and the Achaete-Scute Complex (As-c). Da and As-c transcriptionally autoregulate and thus form two positive feedback loops [56].

S. cerevisiae cells growing on galactose could benefit from bistability on a single-cell and population level. A bistable circuit can produce a decisive response to a slow variation in the stimulus [52]. This decoupling ensures that the abrupt change in the system's output is not dependent on the rate of change of the stimulus and is instead an intrinsic property of the circuit's dynamical system. In addition, bimodality due to an underlying bistability can produce stable lineages of cells with a memory of previous environmental conditions. As a consequence of hysteresis, cells with a history of the stimulus will respond differently to a second exposure due to a shift in the threshold of deactivation. This epigenetic memory of previous environments can fine-tune the switching threshold and provide an additional source of cell-to-cell heterogeneity in the perception of the stimulus.

There are also several potential advantages of bimodality at a population level. For example, significant single-cell phenotypic variation, generated by bimodality, can serve as a bet-hedging strategy for microbial populations in uncertain environments [7, 57]. Since *S. cerervisiae* grows poorly even in the presence of high concentrations of galactose and risks accumulation of the toxic intermediate galactose-1-phosphate, the bimodal response may serve as a population strategy to weigh the ener-

getic costs and benefits of activating the GAL regulon [42]. Another intriguing possibility is whether bimodality establishes a division-of-labor in which the high population metabolizes galactose and produces a byproduct that is used by the low population [58].

Feedback loops are ubiquitous in biological systems, and dissecting their precise quantitative roles is a crucial step for unraveling the organizational principles of cellular decision-making. While a single transcriptional positive feedback loop can generate bistability with cooperativity and precise parameter tuning, this study suggests that a single noncooperative positive feedback loop with sequestration can generate bistability and this bistability parameter region can be significantly augmented by the addition of a second positive feedback loop. These insights will be essential for pinpointing the operational principles of switch-like cellular responses, in addition to suggesting rules for designing robust synthetic circuits.

Materials and Methods

Strains

All plasmids used in this study were derived from a set of yeast single integration vectors constructed in the lab of Wendell Lim (UCSF). These vectors contain markers and targeting sequences for the *LEU2*, *HIS3*, *TRP1* and *URA3* loci. These vectors were linearized for transformation by digesting with PmeI and transformed using standard techniques. Promoters were cloned between the PspOMI and XhoI restriction sites and coding sequences were inserted between the XhoI and BamHI sites. These plasmids contained an *ADH1* terminator downstream of BamHI site. All strains were haploid with the exception of MA0182 and wild-type diploid [20]. In the haploid backgrounds, rtTA-M2 was expressed from a medium strength variant of the *TEF* promoter, *TEFm4* [43, 59]. Gene deletions were verified using polymerase chain reaction. A functional test for constitutive P$_{GAL10}$Venus expression in the absence of galactose was also used to verify successful deletion of *GAL80*. Strains are listed in Table SII. The sequences for the *GAL3*, *GAL10* and *GAL80* promoters were 1017, 646 and 283 base pairs upstream of the start codons, respectively. The *TET* promoter consisted

of a region of the *CYC1* promoter and two TetR operator binding sites [60]. The synthetic single *GAL4* binding site promoter, $P_{CYC1\text{-}G4BS}$, consisted of a binding site from the *GAL7* promoter (CGGACAACTGTTGACCG) upstream of the *CYC1* core promoter.

Growth conditions and flow cytometry

Cells were grown in appropriate dropout media supplemented with 2% filter-sterilized raffinose at 30°C. In 2% raffinose media supplemented with zero or small amounts of galactose, cell divisions occurred approximately every three hours during exponential growth phase. Steady-state measurements were performed after a 20 hour induction period. Cells were induced for 30 hours for hysteresis experiments as explained in Section S2.1. OD_{600} (cell density) was maintained below 0.1 to prevent significant changes in the galactose concentration for the duration of the experiment. Flow cytometry measurements were made using a MACSQuant VYB (Miltenyi Biotec) or LSRII analyzer (BD Biosciences). For both instruments, a blue (488 nm) laser was used to excite YFP. Emission was detected on the MACSQuant or LSRII using a 525/50 nm and 530/30 nm filter, respectively. At least 10,000 cells were collected for each measurement.

Analysis of flow cytometry distributions

Bimodality classification

Flow cytometry distributions were analyzed using a Gaussian mixture model algorithm (GMM, MATLAB) [61]. The GMM assumes that the data is a mixture distribution where the probability density function is a linear combination with coefficients that sum to one ($\xi_1 + \xi_2 = 1$).

$$f(x) = \xi_1 N_1 \left(\mu_1, \sigma_1 \right) + \xi_2 N_2 \left(\mu_2, \sigma_2 \right).$$

The parameters for the GMM include the means, μ_1, μ_2, standard deviations, σ_1, σ_2 and mode weights ξ_1, ξ_2. A distribution was categorized bimodal if the following conditions were true

$$|\mu_1 - \mu_2| > 2\max(\sigma_1, \sigma_2),$$

$$\min(\xi_1, \xi_2) > 0.1.$$

Activation responses

Activation responses for bimodal transitions were analyzed using the fraction of high expressing cells (F_H). The threshold was set to the minimum separating the two local maxima. $F_H = \frac{n_H}{n_{tot}}$ where n_H and n_L are the number of high and low expressing cells, respectively ($n_{tot} = n_H + n_L$). The activation level for a graded response was quantified using the normalized mean fluorescence level (M_Y),

$$M_Y = \frac{(\log_{10}(Y) - \min(\log_{10}(Y)))}{(\max(\log_{10}(Y)) - \min(\log_{10}(Y)))}.$$

Quantitative real-time PCR

Total RNA was isolated using a YeaStar RNA Kit (Zymo Research Corp.). Oligonucleotides for quantitative real-time PCR (qPCR) were designed using Integrated DNA Technologies PrimeTime qPCR assay. 500 nanograms total RNA was reverse-transcribed using the iScript cDNA synthesis kit (Bio-Rad). The reaction mix contained 5 μl of SsoFast Probes SuperMix (Bio-Rad), 0.5 μl of primer probe corresponding to 250 nM primers and 125 nM probe (20X stock) and 0.5 μl cDNA. Three technical replicates for each sample were analyzed using the CFX96 real-time PCR machine (Bio-Rad). Relative expression levels were determined by the $2^{(-\Delta\Delta C_t)}$ method [62]. Each sample was normalized by the C_t geometric mean for the reference genes, *ACT1* and *UBC6* [63].

Computational modeling

Code for mathematical modeling was written in MATLAB (Mathworks) and Mathematica (Wolfram Research).

Bifurcation points

We identified turning, fold and saddle-node bifurcation points that can create bistability by computing the values of α_{gal} that caused a real eigenvalue of the Jacobian matrix to change from negative to positive, producing a singular Jacobian matrix at the point where the real part of the eigenvalue equaled zero. The bifurcation parameter $(\lambda = \alpha_{gal})$ appeared linearly in the polynomial equations for the equilibrium concentrations of Gal4p. To satisfy the conditions of a singular Jacobian matrix and equilibrium, there were two equations in two unknowns using the Gal4p polynomial $(x = \text{Gal4p})$

$$f(x) + \lambda g(x) = 0,$$

$$f'(x) + \lambda g'(x) = 0.$$

We solved the system of equations using the Sylvester resultant [64]. This resultant provides conditions for the coefficients of two polynomials of a single variable to have a root in common. Sylvester matrices A and B contained the coefficients of f, f' and g, g', respectively. The dimensions of A and B were $(d_1 + d_2)$ x $(d_1 + d_2)$ where d_1, d_2 are the degrees of highest polynomial of either f or g and correspondingly f' or g', respectively. The bifurcation points were computed by solving the generalized eigenvalue problem $(A + \lambda B)\phi = 0$.

Acknowledgments

Author contributions

OSV, RMM and HES conceived the research and OSV did the experiments, analyzed the data, constructed the model, did the analysis and wrote the manuscript with substantial input from RMM and HES.

Supplementary Information

S2.1 Distinguishing dilution memory from a history-dependent response

YFP is highly stable and predominantly decreases through cell dilution [65]. As a consequence, activation of P_{GAL10}YFP is faster than deactivation, and distributions of cells from E_H and E_L will inevitably differ until cells equilibrate to a new steady-state in the second set of environments (E_1, ..., E_n). We estimated the amount of time and hence the number of cell divisions necessary to distinguish dilution memory from a history-dependent response (Fig. 2.2).

In the presence of 2% galactose, the steady-state YFP fluorescence expressed from the *GAL10* promoter was approximately 78% of YFP fluorescence expressed from the *TDH3* promoter after autofluorescent background subtraction (Supplementary Fig. 2.1A). There are approximately 169,000 Tdh3 proteins present in glucose conditions in a haploid *S. cerevisiae* background [66], corresponding to 131,820 Gal10 proteins (assuming promoter strength is proportional to the number of molecules). Therefore, the concentration of Gal10p is 7.5 μM at full galactose induction [67]. As a lower bound, we assumed that 150 molecules of YFP (8.6 nM) was indistinguishable from the autofluorescence background using flow cytometry [68]. Therefore, the number of cell divisions required to dilute YFP from full induction to background is $\log_2(7.5) - \log_2(0.0086) = 9.8$. In minimal dropout media supplemented with 2% raffinose, cells doubled approximately every three hours during exponential phase, which corresponds to 30 hours to distinguish dilution memory from a history-dependent response.

S2.2 Characterization of the *GAL3* feedback loop on the bimodal response

We found that bimodality persisted in the absence of the *GAL3* feedback loop for a range of wild-type (WT) *GAL3* levels as shown in Fig. 2.3A-4. These results are different from a previous study that attributed the observed bimodality of the GAL network to the activity of the *GAL3* feedback loop [20]. This study used a diploid *GAL3* feedback loop deletion strain where Gal3p was constitutively expressed with a *TET* inducible promoter. Using fluorescent Gal3 fusion proteins, the authors identified 50 ng/ml dox as equivalent to 80% of the WT *GAL3* levels induced with 0.5%
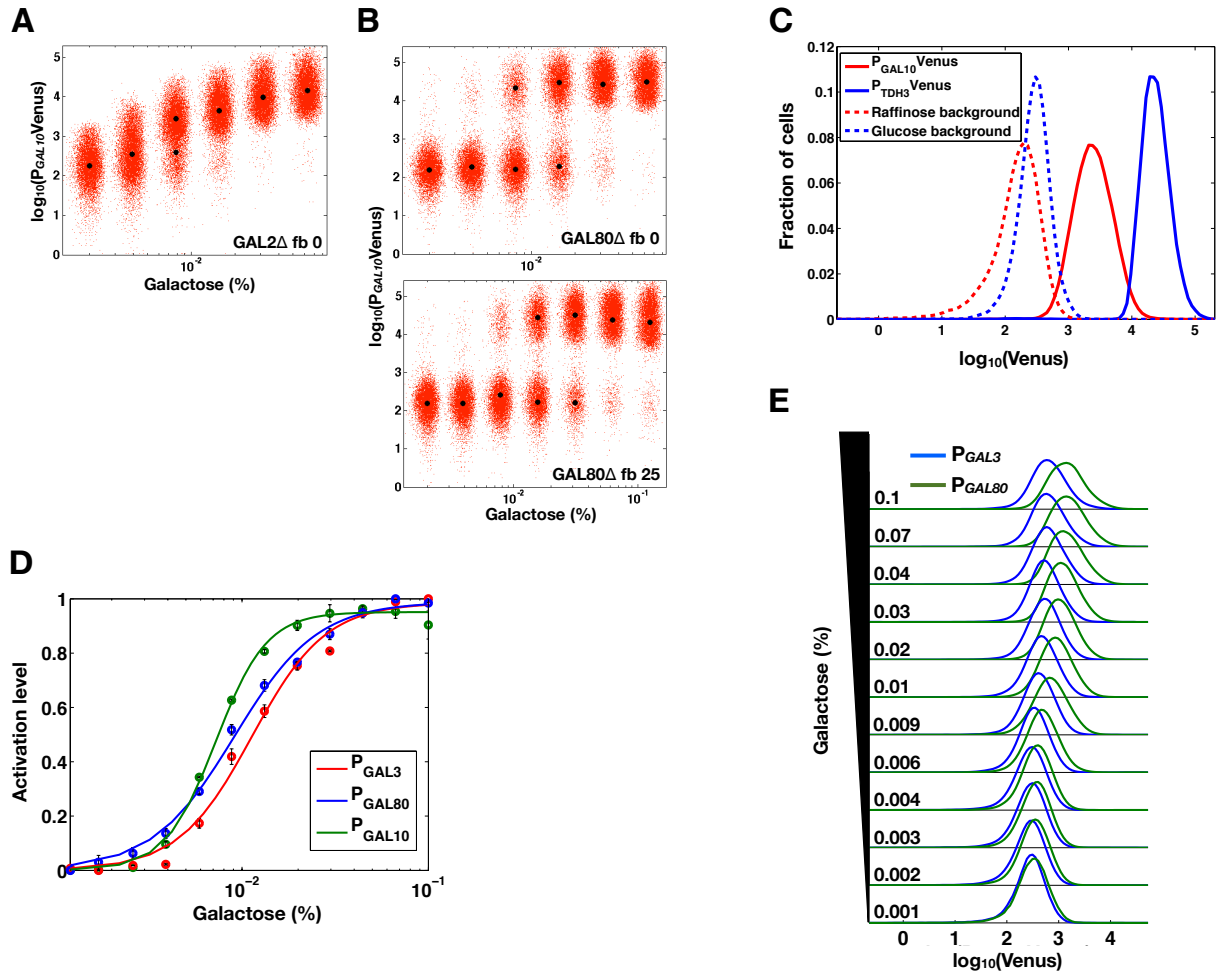
Supplementary Figure 2.1: Comparison of promoter strengths and ultrasensitivity. Venus (YFP) fusions to the *TDH3*, *GAL3*, *GAL10* and *GAL80* promoters in a wild-type (WT) background (P_{TDH3}Venus, P_{GAL3}Venus, P_{GAL10}Venus and P_{GAL80}Venus). **(A)** Comparison of *GAL10* and *TDH3* promoter strengths. Promoter were compared after subtracting the corresponding autofluoresence background (solid red and blue histograms). P_{GAL10}Venus and P_{TDH3}Venus were grown separately in 2% raffinose + 2% galactose or 2% glucose. The autofluoresence background values were obtained from a wild-type W303a strain lacking a fluorescent reporter grown separately in 2% raffinose or 2% glucose media (dashed red and blue histograms) **(B)** Activation level represents the fraction of high expressing cells for P_{GAL10} and the normalized mean of unimodal distributions for P_{GAL3} and P_{GAL80} (M_Y, see Materials and methods). Lines are fits of the data to Hill functions with Hill coefficients of 3.2, 2.2 and 2 for P_{GAL10}, P_{GAL3} and P_{GAL80}. Error bars represent one standard deviation (n=3). **(C)** Representative flow cytometry distributions of Venus from P_{GAL3} and P_{GAL80} for a range of galactose concentrations at steady-state. Since the *GAL3* and *GAL80* promoters are weaker than the *GAL10* promoter, the flow cytometry gain settings were increased for these strains to detect the full expression range.

galactose.

To further explore the roles of the $GAL3$ feedback loop on the bimodal response, we repeated the experiments from Acar *et al.* using the MA0182 strain. Following the authors' protocol, we observed bimodality in P_{GAL1}YFP expression after an induction of 27 hours for 0.004% galactose in the absence of doxycycline (dox) (Supplementary Fig. 2.2A). A Gaussian mixture model (GMM) was used to classify bimodality (see Materials and Methods). Using this criteria, these data showed the $GAL3$ feedback loop was not necessary for bimodality for some range of $GAL3$ levels (Supplementary Fig. 2.2B).

The galactose dose response was next measured for different $GAL3$ levels by inducing MA0182 with a range of galactose and dox concentrations (Supplementary Fig. 2.2A). These data showed that MA0182 was bimodal for at least one galactose concentration between 0-25 ng/ml dox (Supplementary Fig. 2.2B). However, bimodality was not detected for 50 ng/ml dox.

We compared $GAL3$ mRNA levels to WT $GAL3$ expression using quantitative real-time PCR (qPCR). According to these results, 50 ng/ml dox corresponded to approximately 150% $GAL3$ levels relative to WT induced with 0.5% galactose (Supplementary Fig. 2.2C). These results indicated that WT $GAL3$ expression in MA0182 was between 0 ng/ml (36%) and approximately 35 ng/ml dox (100%). Acar *et al.* stated that MA0182 displayed a graded response for 5-300% of $GAL3$ levels with respect to WT. In our experiments, the lower bound for $GAL3$ levels in MA0182 was 36% of maximal WT levels due to leakiness of the TET inducible promoter system.

In summary, MA0182 exhibited a bimodal response for a range of WT $GAL3$ expression levels and was graded when Gal3p was overexpressed. This transformation of the GAL dose response from bimodal to graded by tuning the concentration of Gal3p corroborates the importance of comparing feedback loop knockouts at similar operating point(s) to fully understand the contribution of these regulatory connections to a phenotype (Section S2.3) [69].
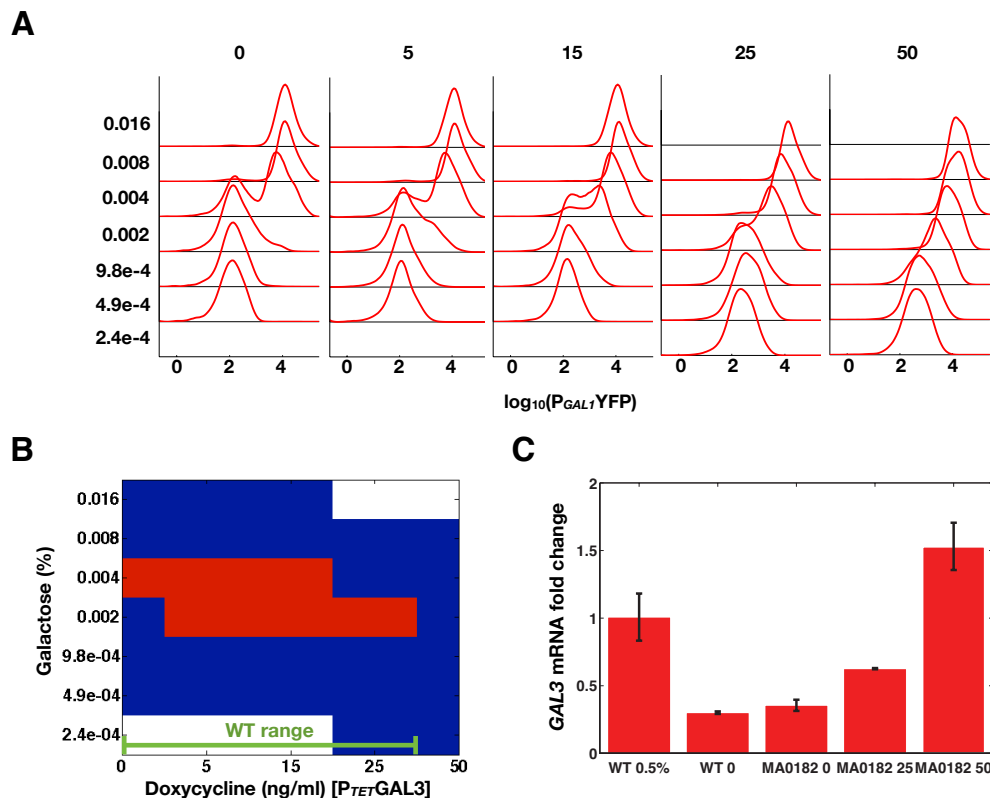
Supplementary Figure 2.2: Experimental characterization of the diploid *GAL3* feedback loop knockout strain MA0182 from [20]. **(A)** Flow cytometry histograms of YFP fluorescence for a range of doxycycline (dox, horizontal axis) and galactose (percent, vertical axis) concentrations. **(B)** Representation of flow cytometry distributions in (A) as bimodal (red) and unimodal (blue) classified using a Gaussian mixture model (see Materials and methods). The concentrations of galactose that yielded bimodal distributions shifted to lower galactose concentrations as the concentration of *GAL3* was increased, qualitatively reflecting the decrease in the bistability region for the *GAL3* feedback deletion model (Fig. 2.5D). The dose response was graded for 50 ng/ml dox. The concentrations of dox that map *GAL3* levels in MA0182 to wild-type (WT) expression are indicated by a green line (0-25 ng/ml dox). **(C)** Quantitative real-time PCR measurements comparing *GAL3* mRNA levels in MA0182 to a diploid WT. This WT strain was induced with 0% and 0.5% galactose and MA0182 was induced with 0, 25 and 50 ng/ml dox. In comparison to WT induced with 0.5% galactose, *GAL3* levels in MA0182 were between 0 (36% with respect to wild-type) and approximately 35 ng/ml dox (100% with respect to WT). Error bars represent one standard deviation (n=3).

S2.3 Comparison of open and closed loop transcriptional circuits

In engineering, closed and open loop systems are frequently compared to determine the advantages of feedback control on performance [14]. Similarly, in biology, a controlled comparison for open and closed loop systems may provide insight about the role of a feedback loop [69]. One approach to creating the open loop system is to delete the gene involved in the loop. However, deleting a gene is an aggressive approach that may significantly shift the operating point of the circuit, making it difficult to attribute the changes in phenotype to the function of the feedback loop. Deleting the coding region of the gene involved in the loop and expressing this gene from a constitutive promoter is a superior approach for evaluating the function of a feedback loop. The constitutive promoter strength is an important parameter to adjust since a comparison of the open and closed loop systems should be made in the neighborhood of the wild-type equilibrium point(s).

Consider a bistable transcriptional circuit modeled by an ordinary differential equation (ODE) that has two stable steady-states for a specific range of an input parameter, u, $\frac{dx}{dt} = u + H(x, \theta) - \gamma x$. We are interested in the role of a positive feedback loop of protein, x. In the closed loop system (wild-type), $H(x, \theta)$ represents transcriptional feedback regulation where

$$H(x, \theta) = \frac{\alpha x^n}{x^n + K^n}.$$

For $u = u_1$, $\frac{dx}{dt} = 0 \Rightarrow x = x_{ei}$ where i corresponds to the particular equilibrium point ($i = 1, 2$ within the bistable parameter regime). Given $u = u_1$ in the bistable region, the open loop system should be evaluated at $\alpha_{OL1} = H(x_{e1}, \theta)\big|_{u=u_1}$ and $\alpha_{OL2} = H(x_{e2}, \theta)\big|_{u=u_1}$, where α_{OL1} and α_{OL2} represents the constitutive (open-loop) production rates. Experimentally mapping the open and closed loop production rates for a range of inputs, $u = u_1, \ldots, u_n$, may be challenging due to a limited number of well-characterized constitutive promoters and restricted dynamic ranges of inducible promoter systems. To circumvent this, an intermediate α'_{OL} can be chosen within the WT expression range

$$\alpha'_{OL} \in [H(\min(x_{ei}), \theta), H(\max(x_{ei}), \theta)] \text{ for } u_1, \ldots, u_n.$$

The caveat for this approximation is that α'_{OL} produces a higher and/or lower open loop expression level compared to WT for each value of u. Using this approach, it is therefore important to check that the role of the feedback does not depend on the specific value α'_{OL} by scanning several values within WT range (Supplementary Fig. 2.2 and Supplementary Fig. 2.3).

S2.4   Model description and steady-state solution

An ODE model of the GAL gene-regulatory circuit was constructed based on the interactions shown in Fig. 2.1. This model was able to provide explanations for experimental data and insights about the interplay of feedback loops. We assumed the following:

- Intracellular galactose concentration is constant.

- Since the *GAL2* feedback is not necessary for bimodality, Gal2p was not modeled for simplicity (Fig. 2.3B-1).

- No distinction was made between Gal1p, Gal1p bound to galactose (Gal1p*) and Gal3p, Gal3 bound to galactose (Gal3p*) since both the galactose bound and unbound forms can function as co-inducers of GAL gene expression, presumably with different affinities [25].

- We did not differentiate between nuclear and cytoplasmic partitioning of the GAL proteins because this is a subject of debate [70, 71, 72].

- Dimerization of Gal4p and Gal80p was not modeled for simplicity [73, 74].

For constant galactose concentrations, conversion of Gal1p, Gal3p into Gal1p*, Gal3p* is a first order reaction. This first order reaction was approximated as a zeroth order reaction using a constant input rate (α_{gal}). The protein concentrations of Gal1p (G1), Gal3p (G3), Gal4p (G4) and Gal80p (G80) were modeled. The Hill coefficients for G1 (n_1), G3 (n_3) and G80 (n_{80}) were estimated as 3, 2 and 2 based on experimental measurements (Supplementary Fig. 2.1B).

A

B
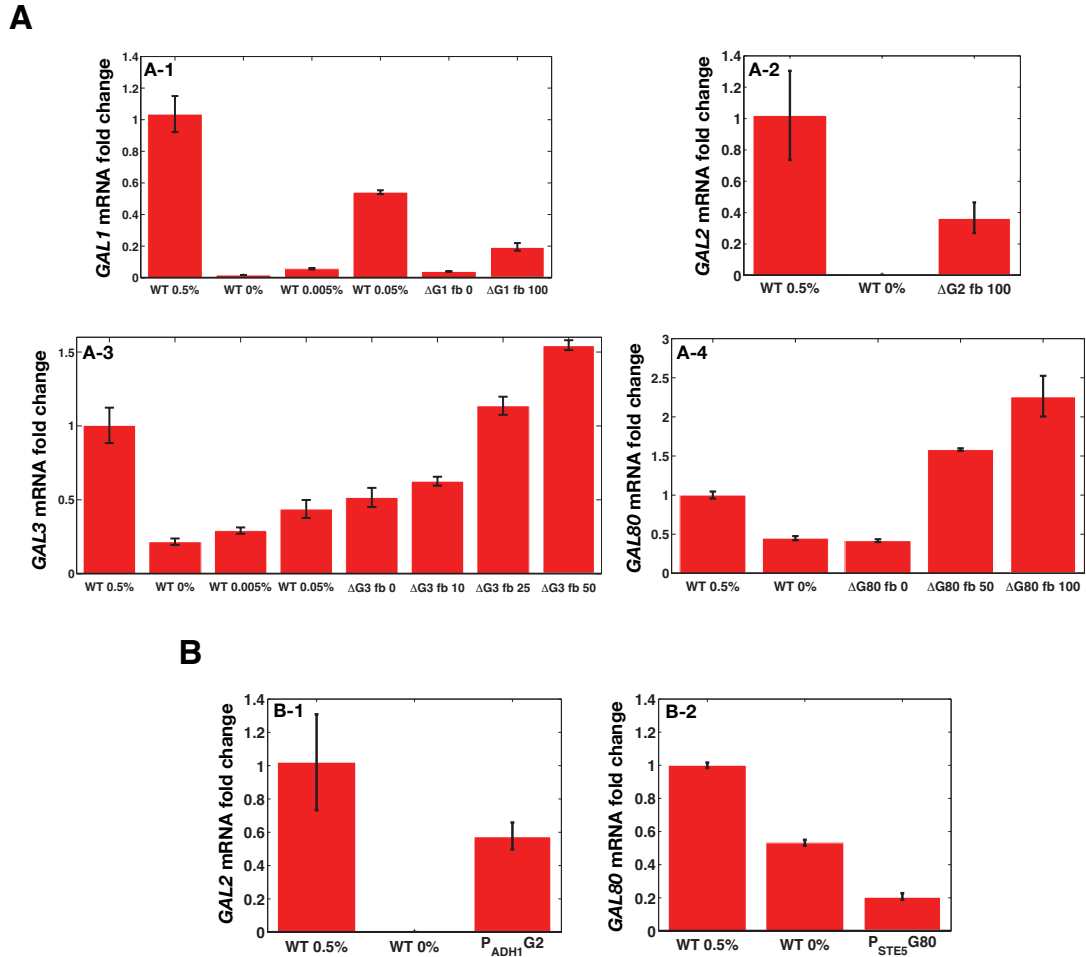
Supplementary Figure 2.3: Quantitative real-time PCR (qPCR) comparing constitutive and wild-type (WT) mRNA levels of *GAL1* (A-1), *GAL2* (A-2), *GAL3* (A-3), *GAL80* (A-4). The mRNA expression level for each gene was compared to the corresponding expression level of this gene in WT induced with 0.5% galactose. **(A)** Comparison of *TET* promoter and WT expression ranges. *GAL1* expressed from the *TET* promoter and induced with 0-100 ng/ml was within the range of WT *GAL1* expression. However, P_{TET}GAL1 induced with 0 and 100 ng/ml dox was overexpressed relative to WT induced with 0% and 0.005% galactose, respectively. P_{TET}GAL2 induced with 100 ng/ml dox corresponded to 37% of saturated WT *GAL2* levels. WT *GAL3* levels corresponded to 0-20 ng/ml dox for *GAL3* expressed from the *TET* promoter. However, P_{TET}GAL3 induced with 10 ng/ml dox was overexpressed relative to 0.05% galactose. P_{TET}GAL80 induced with 0-25 ng/ml dox corresponded to WT *GAL80* expression. **(B)** mRNA levels of *GAL2* (B-1) and *GAL80* (B-2) regulated by the *ADH1* and *STE5* promoters. *GAL2* and *GAL80* levels were approximately 58% and 20% of the corresponding gene in WT induced with 0.5% galactose, respectively. Error bars represent one standard deviation (n=3).

Based on these assumptions, the model that captures the set of critical molecular interactions for

bistability in the wild-type (WT) GAL network is

$$\frac{d[\text{G1}]}{dt} = \epsilon\alpha_{gal} + \alpha_{G1}\left(\frac{[\text{G4}]^{n_1}}{K_{G1}^{n_1} + [\text{G4}]^{n_1}}\right) - k_{f81}[\text{G1}][\text{G80}] + k_{r81}[\text{C81}] - \gamma_{G1}[\text{G1}],$$

$$\frac{d[\text{G3}]}{dt} = \alpha_{gal} + \alpha_{G3}\left(\frac{[\text{G4}]^{n_3}}{K_{G3}^{n_3} + [\text{G4}]^{n_3}}\right) - k_{f83}[\text{G3}][\text{G80}] + k_{r83}[\text{C83}] - \gamma_{G3}[\text{G3}],$$

$$\frac{d[\text{G4}]}{dt} = \alpha_{G4} - k_{f84}[\text{G4}][\text{G80}] + k_{r84}[\text{C84}] - \gamma_{G4}[\text{G4}],$$

$$\frac{d[\text{G80}]}{dt} = \alpha_{oG80} + \alpha_{G80}\left(\frac{[\text{G4}]^{n_{80}}}{K_{G80}^{n_{80}} + [\text{G4}]^{n_{80}}}\right) - k_{f81}[\text{G1}][\text{G80}] + k_{r81}[\text{C81}]$$

$$- k_{f83}[\text{G3}][\text{G80}] + k_{r83}[\text{C83}] - k_{f84}[\text{G4}][\text{G80}] + k_{r84}[\text{C84}] - \gamma_{G80}[\text{G80}],$$

$$\frac{d[\text{C81}]}{dt} = k_{f81}[\text{G1}][\text{G80}] - k_{r81}[\text{C81}] - \gamma_{C81}[\text{C81}],$$

$$\frac{d[\text{C83}]}{dt} = k_{f83}[\text{G3}][\text{G80}] - k_{r83}[\text{C83}] - \gamma_{C83}[\text{C83}],$$

$$\frac{d[\text{C84}]}{dt} = k_{f84}[\text{G4}][\text{G80}] - k_{r84}[\text{C84}] - \gamma_{C84}[\text{C84}].$$

Using the quasi-steady-state assumption, the concentrations of the complexes, Gal1p-Gal80p (C81),

Gal3p-Gal80p (C83) and Gal4p-Gal80p (C84) reached their respective equilibria significantly faster

the dynamics of G1, G3, G4 and G80 ($\frac{d[\text{C81}]}{dt} = \frac{d[\text{C83}]}{dt} = \frac{d[\text{C84}]}{dt} = 0$), yielding

$$[\text{C81}] = \frac{k_{f81}[\text{G1}][\text{G80}]}{k_{r81} + \gamma_{C81}}, \quad [\text{C83}] = \frac{k_{f83}[\text{G3}][\text{G80}]}{k_{r83} + \gamma_{C83}}, \quad [\text{C84}] = \frac{k_{f84}[\text{G4}][\text{G80}]}{k_{r84} + \gamma_{C84}}.$$

This assumption was used to simplify the system of equations to the following four ODEs

$$\frac{d[\text{G1}]}{dt} = \alpha_{gal}\epsilon + \alpha_{G1}\left(\frac{[\text{G4}]^{n_1}}{K_{G1}^{n_1}[\text{G4}]^{n_1}}\right) + \omega[\text{G1}][\text{G80}] - \gamma_{G1}[\text{G1}],$$

$$\frac{d[\text{G3}]}{dt} = \alpha_{gal} + \alpha_{G3}\left(\frac{[\text{G4}]^{n_3}}{K_{G3}^{n_3} + [\text{G4}]^{n_3}}\right) + \delta[\text{G3}][\text{G80}] - \gamma_{G3}[\text{G3}],$$

$$\frac{d[\text{G4}]}{dt} = \alpha_{G4} + \beta[\text{G80}][\text{G4}] - \gamma_{G4}[\text{G4}],$$

$$\frac{d[\text{G80}]}{dt} = \alpha_{oG80} + \alpha_{G80}\left(\frac{[\text{G4}]^{n_{80}}}{K_{G80}^{n_{80}} + [\text{G4}]^{n_{80}}}\right) + \omega[\text{G1}][\text{G80}] + \delta[\text{G3}][\text{G80}] + \beta[\text{G80}][\text{G4}] - \gamma_{G80}[\text{G80}],$$

where

$$\omega = \frac{k_{r81}k_{f81}}{k_{r81} + \gamma_{C81}} - k_{f81}, \quad \delta = \frac{k_{r83}k_{f83}}{k_{r83} + \gamma_{C83}} - k_{f83}, \quad \beta = \frac{k_{r84}k_{f84}}{k_{r84} + \gamma_{C84}} - k_{f84}.$$

At steady-state, $\frac{d[G1]}{dt} = \frac{d[G3]}{dt} = \frac{d[G4]}{dt} = \frac{d[G80]}{dt} = 0$ and the equilibrium concentrations are

$$\text{G1}_e = \frac{-\epsilon\alpha_{gal} - H_{G1}(\text{G4}_e, \theta_{G1})}{\omega\text{G80}_e - \gamma_{G1}},$$

$$\text{G3}_e = \frac{-\alpha_{gal} - H_{G3}(\text{G4}_e, \theta_{G3})}{\delta\text{G80}_e - \gamma_{G1}},$$

$$\text{G80}_e = \frac{-\alpha_{G4} + \gamma_{G4}\text{G4}_e}{\beta\text{G4}_e},$$

where $\text{G1}_e, \text{G3}_e, \text{G4}_e$ and G80_e are the equilibrium values of G1, G3, G80 and G4. G4_e was determined by computing the roots of a eleventh order polynomial

$$a_0 + a_1\text{G4}_e + \cdots + a_{11}\text{G4}_e^{11} = 0,$$

where the coefficients, a_i, are functions of the model parameters. The *GAL1*, *GAL3* and *GAL80* feedback deletion models listed in Section S2.6 were solved by applying the same procedure. The stability of the equilibrium points was determined by computing the eigenvalues of the Jacobian matrix of the system of equations [14].
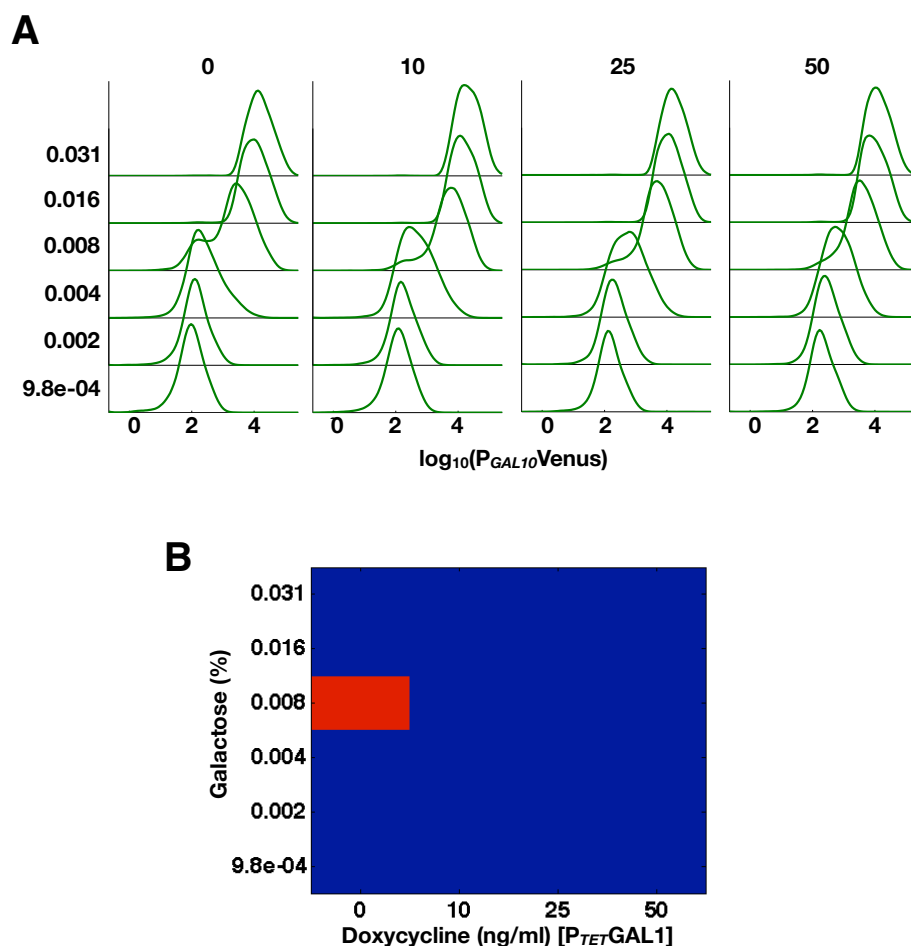
Supplementary Figure 2.4: Experimental characterization of the *GAL1* feedback loop knockout strain (GAL1Δ fb). **(A)** Flow cytometry histograms of P$_{GAL10}$Venus for a range of doxycycline (dox, horizontal axis) and galactose (percent, vertical axis). **(B)** Representation of flow cytometry data in **A** as bimodal (red) and unimodal (blue) determined by a Gaussian mixture model (see Materials and methods). Bimodality was detected for 0 ng/ml dox and vanished for 10, 25 and 50 ng/ml dox.

S2.5 Estimation of model parameters

S2.5.1 Parameter set I

Parameters for the model were estimated from experimental measurements and previous studies (Table SI). *GAL1* and *GAL10* share a bidirectional promoter (P$_{GAL1-10}$). As a consequence, these genes exhibit highly similar galactose induction responses. The *GAL3* and *GAL80* promoters each have a single Gal4p binding site and are produced at a basal rate in the absence of galactose. Multiple Gal4p binding sites in the *GAL2*, *GAL7* and *GAL1-10* promoters stabilize Gal80p dimers

A

B
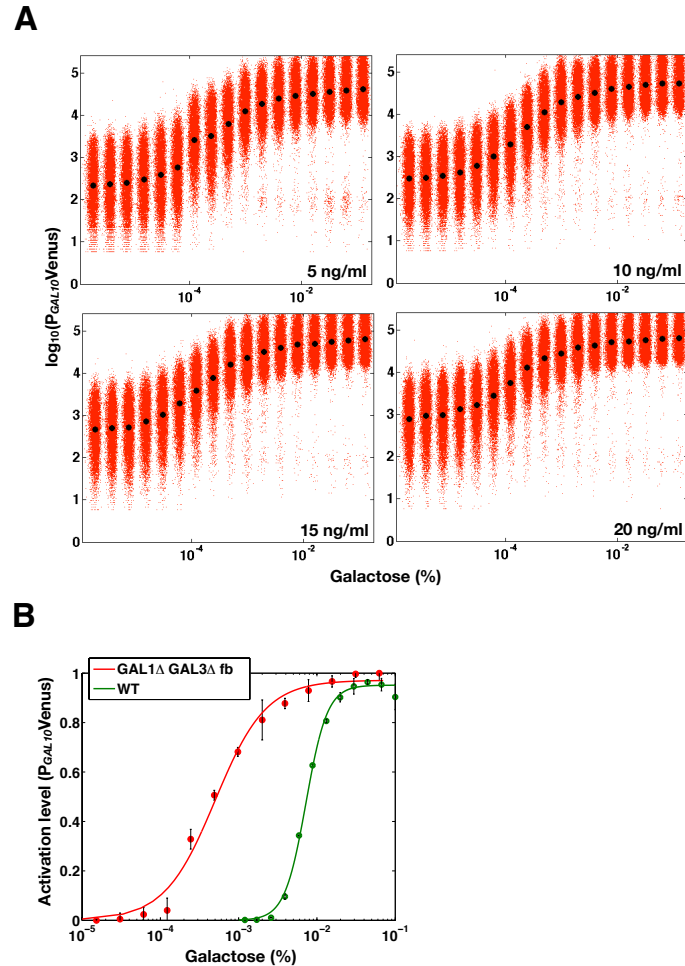
Supplementary Figure 2.5: Deletion of *GAL1* and the *GAL3* feedback loop (GAL1Δ GAL3Δ fb) produced a graded response irrespective of the concentration of *GAL3*. Bimodality persists in the absence of the individual *GAL2* and *GAL80* feedback loops for a wide range of constitutive *GAL2* and *GAL80* levels. **(A)** Steady-state flow cytometry measurements of P_{GAL10}Venus in GAL1Δ GAL3Δ fb cells where *GAL3* was expressed from a *TET* promoter induced with 5, 10, 15 and 20 ng/ml doxycycline (dox). These concentrations of dox correspond to wild-type *GAL3* levels (Supplementary Fig. 2.3A-3). These measurements were taken on an LSRII analyzer. **(B)** *GAL2* feedback deletion (GAL2Δ fb) displayed bimodality in the absence of doxycycline (dox). **(C)** *GAL80* feedback deletion (GAL80Δ fb) exhibited bimodal distributions for 0 and 25 ng/ml dox. These concentrations of dox correspond to 40% and 100% of fully induced WT *GAL80* mRNA levels, respectively. **(D)** Steady-state activation responses of P_{GAL10}Venus in the WT and GAL1Δ GAL3Δ fb. The Hill coefficient for the WT was approximately 3 whereas the Hill coefficient for GAL1Δ GAL3Δ fb was approximately 1.3. Each data point for GAL1Δ GAL3Δ fb represents the normalized mean of fluorescence (M_Y, see Materials and methods) and the error bars represent one standard deviation (n=3). Each data point for the WT represents mean of the fraction cells in the high expression state and the error bars represent one standard deviation (n=3).
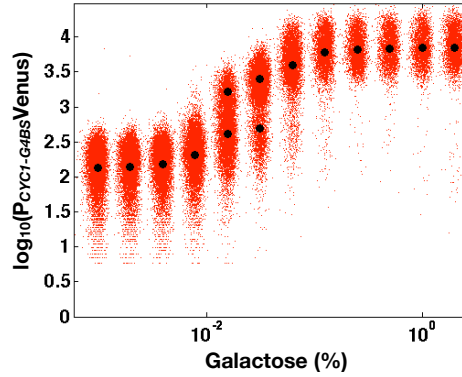
Supplementary Figure 2.6: GAL bimodal response does not require multiple *GAL4* binding sites. A synthetic GAL regulated promoter fusion to Venus with a single *GAL4* binding site was bimodal for two galactose concentrations at steady-state. Bimodality was determined using a Gaussian mixture model (GMM, see Materials and methods). Black circles represent the means of the fluorescence distributions.
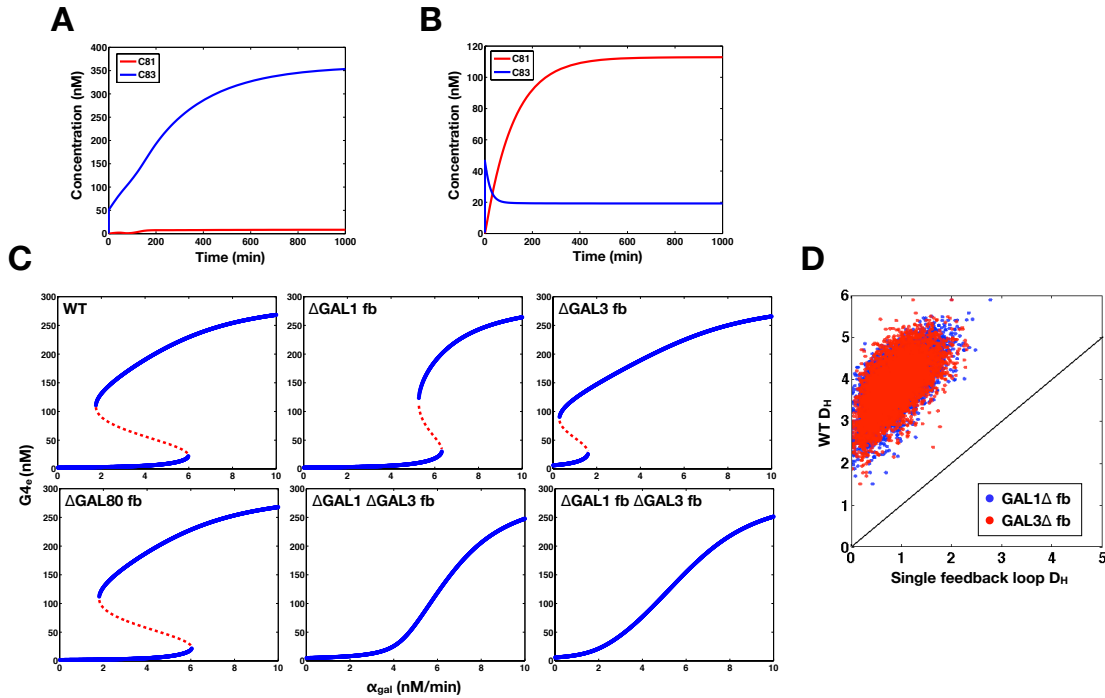
Supplementary Figure 2.7: Parameter set II captures dynamic interplay of Gal1p and Gal3p complex with Gal80p (C81 and C83) and feedback loop knockout experimental results. **(A)** Parameter set I indicates that the complex of Gal3p with Gal80p (C83) dominates transiently and at steady-state compared to C81 (complex of Gal1p with Gal80p). **(B)** Random parameter sampling (see Materials and Methods) was used to identify a new parameter set that exhibits transient dominance of the C83 complex and steady-state dominance of the C81 complex. **(C)** Parameter set II qualitatively matches the feedback loop knockout experimental data showing bistability in all feedback loop deletions except the double deletion of *GAL1* and the *GAL3* feedback loop. **(D)** WT model exhibits a larger range of bistability (D_H) compared to the single positive feedback loop systems (*GAL1* and *GAL3*) across a broad region of parameter space ($C_v = 0.1$). Parameter sets I and II are listed in Table SI.

on DNA, augmenting the strength of repression and the maximum production rate [75]. As a result, promoters with multiple Gal4p binding sites have a significantly larger dynamic range of expression.

Flow cytometry measurements of *GAL3*, *GAL10* and *GAL80* promoter fusions to Venus in response to galactose were used to compare relative promoter strengths and cooperativity. The *GAL3* (P_{GAL3}) and *GAL80* (P_{GAL80}) promoter fusions exhibited a graded response whereas the *GAL10* promoter fusion had a bimodal response as shown in Fig. 2.3A-1. The Hill coefficients for the Gal4p dependent feedback terms were approximated by fitting the means of the graded response distributions (M_Y as described in the Materials and methods) and the fraction of high expressing cells for the bimodal response (P_{GAL10}) to Hill functions.

A Hill function fit to the means of the distributions for P_{GAL3}Venus and P_{GAL80}Venus in response to galactose generated Hill coefficients of 2.2 and 2. Gal4p binds to DNA as a dimer and has been shown to interact cooperatively [73, 76]. Based on these results, we assumed that the Hill coefficients for the *GAL3* and *GAL80* transcriptional feedback terms were two [73, 76].

Fitting the fraction of high expression cells for P_{GAL10} produced a Hill coefficient of approximately 3.2. The *GAL1-10* promoter has four Gal4p binding sites which have been shown to increase cooperativity. Therefore, we set the Hill coefficient of the *GAL1* feedback to three [76]. We note that the main conclusions about the roles of the *GAL1*, *GAL3* and *GAL80* feedback loops do not change if the Hill coefficients of the feedback terms for Gal1p, Gal3p and Gal80p and are set to 4, 1, 1 or 3, 1, 1.

The constitutive and feedback production rates were approximated using the number of proteins per cell [66]. Gal4p is weakly expressed and its constitutive production rate (α_{G4}) was selected to reflect this observation [77]. The mean expression levels for P_{GAL3}Venus and P_{GAL80}Venus were similar in response to galactose as shown in Supplementary Fig. 2.1C. At saturation (0.1% galactose), P_{GAL80}Venus was approximately 15% higher than P_{GAL3}Venus. The production rates, α_{G3}, α_{G80}, α_{oG80}, were chosen to have similar ratios to mirror the experimental measurements. Since Gal1p has been shown to bind to Gal80p with lower affinity than Gal3p, a scaling factor of ϵ was used to modify α_{gal} [26, 32].

Parameter	Description	Units	Parameter Set I*	Parameter set II†
k_{f81}	forward binding rate of Gal1p to Gal80p	$(\text{nM min})^{-1}$	100	100
k_{r81}	unbinding rate of Gal1p from Gal80p	min^{-1}	1500	2500
k_{f83}	forward binding rate of Gal3p to Gal80p	$(\text{nM min})^{-1}$	100	100
k_{r83}	unbinding rate of Gal3p from Gal80p	min^{-1}	1	462
k_{f84}	forward binding rate of Gal4p to Gal80p	$(\text{nM min})^{-1}$	100	100
k_{r84}	unbinding rate of Gal4p from Gal80p	min^{-1}	25	1300
α_{G1}	Gal1p production rate	nM min^{-1}	15	35
α_{G3}	Gal3p production rate	nM min^{-1}	0.9	8
α_{G4}	Gal4p production rate	nM min^{-1}	0.2	3.6
α_{oG80}	Basal Gal80p production rate	nM min^{-1}	0.6	5.9
α_{G80}	Gal80p production rate	nM min^{-1}	0.9	9
K_{G1}	$GAL1$ transcriptional feedback threshold	nM	8	86.7
K_{G3}	$GAL3$ transcriptional feedback threshold	nM	8	64.9
K_{G80}	$GAL80$ transcriptional feedback threshold	nM	2	1.5
n_1	$GAL1$ Hill coefficient	dimensionless	3	3
n_3	$GAL3$ Hill coefficient	dimensionless	2	2
n_{80}	$GAL80$ Hill coefficient	dimensionless	2	2
γ_{G1}	Gal1p degradation rate	min^{-1}	0.004	0.0263
γ_{G3}	Gal3p degradation rate	min^{-1}	0.004	0.004
γ_{G4}	Gal4p degradation rate	min^{-1}	0.004	0.0119
γ_{G80}	Gal80p degradation rate	min^{-1}	0.004	0.0073
γ_{C81}	Gal1p-Gal80p (C81) degradation rate	min^{-1}	0.004	0.0084
γ_{C83}	Gal3p-Gal80p (C83) degradation rate	min^{-1}	0.004	0.0527
γ_{C84}	Gal4p-Gal80p (C84) degradation rate	min^{-1}	0.004	0.0177
ϵ	scaling factor	dimensionless	0.1	1.02
α_{G1s}	constant Gal1p production rate	nM min^{-1}	0.1	0.1
α_{G3s}	constant Gal3p production rate	nM min^{-1}	0.1	6
α_{G80s}	constant Gal80p production rate	nM min^{-1}	1.5	13.5

Supplementary Table I: Description of model parameters used in this study. *Original parameter set estimated as described in Section S2.5 (Fig. 2.4 and Fig. 2.5). †New parameter set obtained by random parameter sampling (Latin hypercube method) that captures the dynamic interplay of Gal1p and Gal3p [34].

Forward binding rates (k_{f83}, k_{f81} and k_{f84}) were estimated using the limits of diffusion. The dissociation rates (k_{r83}, k_{r81}, k_{r84}) were free parameters with the requirement that $k_{r81} \gg k_{r83}$ [26, 32]. The protein concentrations of Gal1, Gal3, Gal4, Gal4 and the complexes C81, C83 and C84 were assumed to degrade linearly at approximately the rate of cell division.

S2.5.2   Parameter set II

To identify parameter sets that qualitatively matched the previously reported dynamic switch response of Gal1p and Gal3p [34], 10,000 parameter sets were sampled uniformly in linear scale in the 22-dimensional parameter space, using the Latin hypercube sampling method [45]. The following parameter ranges were used: 10-160 (nM min)$^{-1}$ for the forward binding constants (k_{f81}, k_{f83} and k_{f84}), 1-5000 min^{-1} for the dissociation constants (k_{f81}, k_{f83} and k_{f84}), 0.0035-0.06 min^{-1} for the degradation rates (γ_{G1}, γ_{G3}, γ_{G80}, γ_{G4}, γ_{C81}, γ_{C83} and γ_{C84}), 0.01-100 nM for the EC$_{50}$ values in the Hill functions (K_{G1}, K_{G3} and K_{G80}), 0.1-40 nM min^{-1} for α_{G1}, 0.1-10 nM min^{-1} for α_{G3}, α_{oG80} and α_{G80}, 0.1-5 nM min^{-1} for α_{G4} and 0.01-2 for ϵ. The constitutive rates for the feedback knockouts were fixed at 0.1, 0.1 and 1.5 nM min^{-1} for α_{G1s}, α_{G3s} and α_{G80s}, respectively. D$_{\mathrm{H}}$ was computed for each parameter set and for each of the five models (WT, GAL1Δ fb, GAL3Δ fb, GAL80Δ fb and GAL1Δ fb GAL3Δ fb). First, these parameter sets were filtered based on the presence of bistability. Second, the subset of parameter sets that satisfied these constraints were simulated and the relative concentrations of C81 and C83 were calculated at an initial (10 min) and delayed (500 min) time point by simulation of the full WT model (7-state) before applying the quasi-steady-state assumption.

S2.6   Feedback loop deletion models

The individual *GAL1*, *GAL3*, *GAL80* and combined *GAL1* and *GAL3* feedback deletions were obtained by replacing the appropriate Hill functions representing transcriptional regulation by Gal4p with a constant or equivalently setting the appropriate thresholds in the Hill functions, K_{Gx}, $x = 1, 3, 80$ to zero. In the GAL80Δ fb model, the basal and constitutive production rate were lumped

into one parameter, α_{G80s}. The GAL1Δ GAL3Δ fb model was obtained from the GAL1Δ fb GAL3Δ fb model by setting $\alpha_{G1s} = 0$ and $\epsilon = 0$. The set of ordinary differential equations to model the five feedback loop knockout topologies are as follows.

S2.6.1 *GAL1* feedback deletion (GAL1Δ fb)

$$\frac{d[\text{G1}]}{dt} = \epsilon\alpha_{gal} + \alpha_{G1s} + \omega[\text{G1}][\text{G80}] - \gamma_{G1}[\text{G1}],$$

$$\frac{d[\text{G3}]}{dt} = \alpha_{gal} + \alpha_{G3}\left(\frac{[\text{G4}]^2}{K_{G3}^2 + [\text{G4}]^2}\right) + \delta[\text{G3}][\text{G80}] - \gamma_{G3}[\text{G3}],$$

$$\frac{d[\text{G4}]}{dt} = \alpha_{G4} + \beta[\text{G80}][\text{G4}] - \gamma_{G4}[\text{G4}],$$

$$\frac{d[\text{G80}]}{dt} = \alpha_{oG80} + \alpha_{G80}\left(\frac{[\text{G4}]^2}{K_{G80}^2 + [\text{G4}]^2}\right) + \omega[\text{G1}][\text{G80}] + \delta[\text{G3}][\text{G80}] + \beta[\text{G80}][\text{G4}] - \gamma_{G80}[\text{G80}],$$

S2.6.2 *GAL3* feedback deletion (GAL3Δ fb)

$$\frac{d[\text{G1}]}{dt} = \epsilon\alpha_{gal} + \alpha_{G1}\left(\frac{[\text{G4}]^3}{K_{G1}^3 + [\text{G4}]^3}\right) + \omega[\text{G1}][\text{G80}] - \gamma_{G1}[\text{G1}],$$

$$\frac{d[\text{G3}]}{dt} = \alpha_{gal} + \alpha_{G3s} + \delta[\text{G3}][\text{G80}] - \gamma_{G3}[\text{G3}],$$

$$\frac{d[\text{G4}]}{dt} = \alpha_{G4} + \beta[\text{G80}][\text{G4}] - \gamma_{G4}[\text{G4}],$$

$$\frac{d[\text{G80}]}{dt} = \alpha_{oG80} + \alpha_{G80}\left(\frac{[\text{G4}]^2}{K_{G80}^2 + [\text{G4}]^2}\right) + \omega[\text{G1}][\text{G80}] + \delta[\text{G3}][\text{G80}] + \beta[\text{G80}][\text{G4}] - \gamma_{G80}[\text{G80}],$$

S2.6.3 *GAL80* feedback deletion (GAL80Δ fb)

$$\frac{d[\text{G1}]}{dt} = \epsilon\alpha_{gal} + \alpha_{G1}\left(\frac{[\text{G4}]^3}{K_{G1}^3 + [\text{G4}]^3}\right) + \omega[\text{G1}][\text{G80}] - \gamma_{G1}[\text{G1}],$$

$$\frac{d[\text{G3}]}{dt} = \alpha_{gal} + \alpha_{G3}\left(\frac{[\text{G4}]^2}{K_{G3}^2 + [\text{G4}]^2}\right) + \delta[\text{G3}][\text{G80}] - \gamma_{G3}[\text{G3}],$$

$$\frac{d[\text{G4}]}{dt} = \alpha_{G4} + \beta[\text{G80}][\text{G4}] - \gamma_{G4}[\text{G4}],$$

$$\frac{d[\text{G80}]}{dt} = \alpha_{G80s} + \omega[\text{G1}][\text{G80}] + \delta[\text{G3}][\text{G80}] + \beta[\text{G80}][\text{G4}] - \gamma_{G80}[\text{G80}],$$

S2.6.4 *GAL1* and *GAL3* feedback deletions (GAL1Δ fb GAL3Δ fb)

$$\frac{d[\text{G1}]}{dt} = \epsilon\alpha_{gal} + \alpha_{G1s} + \omega[\text{G1}][\text{G80}] - \gamma_{G1}[\text{G1}],$$

$$\frac{d[\text{G3}]}{dt} = \alpha_{gal} + \alpha_{G3s} + \delta[\text{G3}][\text{G80}] - \gamma_{G3}[\text{G3}],$$

$$\frac{d[\text{G4}]}{dt} = \alpha_{G4} + \beta[\text{G80}][\text{G4}] - \gamma_{G4}[\text{G4}],$$

$$\frac{d[\text{G80}]}{dt} = \alpha_{oG80} + \alpha_{G80}\left(\frac{[\text{G4}]^2}{K_{G80}^2 + [\text{G4}]^2}\right) + \omega[\text{G1}][\text{G80}] + \delta[\text{G3}][\text{G80}] + \beta[\text{G80}][\text{G4}] - \gamma_{G80}[\text{G80}].$$

S2.7 General models of molecular sequestration with positive feedback

We constructed generalizable models of molecular sequestration and positive feedback to examine the relationship between the binding affinity of the activator-repressor pair(s) and the system's region of bistability. We first explored the parameter dependence of a simple model of an activator x that is regulated by a transcriptional repressor z with a Hill coefficient of 1 (noncooperative). In this model, x can sequester z to form an inactive heterodimer, hence generating a positive feedback loop.

Next, we analyzed the steady-state and dynamic properties of systems with two activators, x_1 and x_2 that are each regulated by the transcriptional repressor z and can sequester z into two inactive complexes (c_1 and c_2), thus forming one or two positive feedback loops. In these models, the mechanisms of sequestration and positive feedback are triggered by an input (u) that represents a basal production rate of x, x_1 and x_2.

S2.7.1 Model description for single noncooperative sequestration feedback loop

The three equations that implement a single noncooperative sequestration feedback loop (Supplementary Fig. 2.8A,B) are

$$\frac{dx}{dt} = u + \frac{\alpha K}{K + z} - k_f x z + k_r c - \gamma_x x,$$

$$\frac{dc}{dt} = k_f x z - k_r c - \gamma_c c,$$

$$\frac{dz}{dt} = \alpha_z - k_f x z + k_r c - \gamma_z z.$$

Here, u represents the input. Assuming that $\frac{dc}{dt} = 0$ (quasi-steady-state approximation), the model

was reduced to

$$\frac{dx}{dt} = u + \frac{\alpha K}{K + z} + \beta x z - \gamma_x x,$$

$$\frac{dz}{dt} = \alpha_z + \beta x z - \gamma_z z,$$

where $\beta = k_f \left(\frac{k_r}{k_r + \gamma_c} - 1 \right)$. The parameter values were set to $\alpha_x = 5$ nM min^{-1}, $\alpha_z = 10$ nM min^{-1},

$\gamma_x = \gamma_c = \gamma_z = 0.005$ min^{-1}, $K = 100$ nM, $k_f = 100$ (nM min)$^{-1}$. u and k_r varied within the range

of 0.1-10 nM min^{-1} and 0.1-1000 min^{-1} (Supplementary Fig. 2.8B). Similar to the GAL model, a

bifurcation analysis was performed by computing the roots of the cubic polynomial in z.

S2.7.2 Model description for double sequestration linked feedback loops

The ODE model that represents a double sequestration linked feedback loop system shown in Fig.

2.6A consists of the following equations
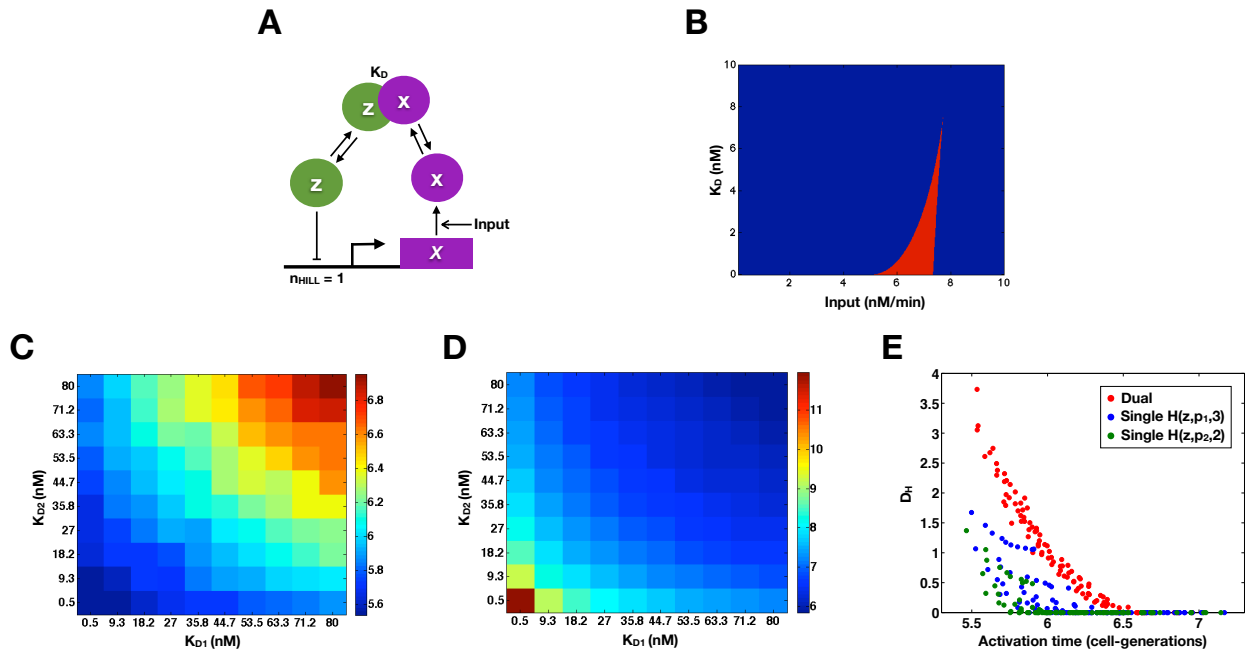
Supplementary Figure 2.8: Molecular sequestration can generate bistability without cooperativity. Relationships between the binding affinities and activation or deactivation response times for the dual feedback loop sequestration model. **(A)** Circuit topology consists of an activator x that can form inactive heterodimers with a transcriptional repressor, z. z transcriptionally represses x with a Hill coefficient of 1 (noncooperative). **(B)** Regions of bistability (red) and monostability (blue) for a set of input and K_D values (binding affinity of x to z). The region of bistability shrinks and eventually disappears as the binding affinity decreases. Model equations and parameter values are listed in Section S2.7. **(C)** Activation response times measured in cell-generations for the double feedback loop sequestration model for different values of K_{D1} and K_{D2}. **(D)** Deactivation response times measured in cell-generations for the double feedback loop sequestration model for different values of K_{D1} and K_{D2}. **(E)** Relationship between activation response times and range of bistability (D_H) for the double positive feedback loop sequestration model for a set of K_{D1} and K_{D2} values. For a fixed nonzero D_H, the double positive feedback loop system could exhibit a faster activation response compared to the single positive feedback loop models.

$$\frac{dx_1}{dt} = u + \frac{\alpha_1 K_1^3}{K_1^3 + z^3} - k_{f1}x_1 z + k_{r1}c_1 - \gamma_1 x_1,$$

$$\frac{dx_2}{dt} = u + \frac{\alpha_2 K_2^2}{K_2^2 + z^2} - k_{f2}x_2 z + k_{r2}c_2 - \gamma_2 x_2,$$

$$\frac{dc_1}{dt} = k_{f1}x_1 z - k_{r1}c_1 - \gamma_{c1}c_1,$$

$$\frac{dc_2}{dt} = k_{f2}x_2 z - k_{r2}c_2 - \gamma_{c2}c_2,$$

$$\frac{dz}{dt} = \alpha_z - k_{f1}x_1 z + k_{r1}c_1 - k_{f2}x_2 z + k_{r2}c_2 - \gamma_z z.$$

Here, u represents the input. Assuming the inactive complexes (c_1 and c_2) approach equilibrium significantly faster than the other species (quasi-steady-state approximation), the system of equations was reduced to

$$\frac{dx_1}{dt} = u + \frac{\alpha_1 K_1^3}{K_1^3 + z^3} + \beta_1 x_1 z - \gamma_1 x_1,$$

$$\frac{dx_2}{dt} = u + \frac{\alpha_2 K_2^2}{K_2^2 + z^2} + \beta_2 x_2 z - \gamma_2 x_2,$$

$$\frac{dz}{dt} = \alpha_z + \beta_1 x_1 z + \beta_2 x_2 z - \gamma_z z,$$

where $\beta_1 = k_{f1}\left(\frac{k_{r1}}{k_{r1}+\gamma_{c1}} - 1\right)$ and $\beta_2 = k_{f2}\left(\frac{k_{r2}}{k_{r2}+\gamma_{c2}} - 1\right)$.

The parameter values were set to $\alpha_1 = \alpha_2 = 5$ nM min^{-1}, $\alpha_z = 10$ nM min^{-1}, $\gamma_1 = \gamma_2 = \gamma_{c1} = \gamma_{c2} = \gamma_z = 0.005$ min^{-1}, $K_1 = K_2 = 100$ nM, $k_{f1} = k_{f2} = 100$ (nM min)$^{-1}$. u, k$_{r1}$ and k$_{r2}$ were each varied over a range of values. The single feedback loop models referred to as the "single n$_{\text{Hill}} = 2$" and the "single n$_{\text{Hill}} = 3$" were obtained by replacing the Hill functions by a constitutive production rate, α_{1s} or α_{2s}. These parameters were set to $\alpha_{1s} = 5$ nM min^{-1}, $\alpha_{2s} = 5$ nM min^{-1} or $\alpha_{1s} = 0.1$ nM min^{-1}, $\alpha_{2s} = 0.1$ nM min^{-1} for the activation or deactivation response time analysis (see below). Similar to the GAL model, a bifurcation analysis was performed by calculating the roots of polynomials in z. The dual, single n$_{\text{Hill}} = 2$ and single n$_{\text{Hill}} = 3$ models were simplified to seventh, fifth and sixth order polynomials in z.

Response time analysis

The activation and deactivation response times were computed by simulation of the full sequestration models described above before applying the quasi-steady-state approximation (six-state ODE model including an output species, y). Total simulation time was 5000 min. The equation for the output species was

$$\frac{dy}{dt} = \frac{\alpha_y K_y^3}{K_y^3 + z^3} - \gamma_y y,$$

and the parameters equaled $\alpha_y = 10$ nM min^{-1}, $K_y = 100$ nM, $\gamma_y = 0.005$ min^{-1}.

Activation response times

For the activation time simulations, $u = 0$ for $t \leq 500$ min and then $u = 10$ for $t > 500$ min. The initial conditions approximated the steady-state concentrations for the low state where $x_{1o} = 0.005$ nM, $x_{2o} = 0.01$ nM, $c_{1o} = 0.12$ nM, $c_{2o} = 2.4$ nM, $z_o = 1998$ nM and $y_o = 0.26$ nM. The time required for y (normalized between 0 and 1) to increase to half its maximum value was computed for each set of K_{D1} and K_{D2} values. In the single feedback loop models, the constitutive production rates of x_1 or x_2 (α_{1s} or α_{2s}) were set to 0.1 nM min^{-1} because this value approximated the Hill functions at equilibrium for $u = 0$.

Deactivation response times

For the deactivation time simulations, $u = 10$ for $t \leq 500$ min and then $u = 0$ for $t > 500$ min. The initial conditions approximated the steady-state concentrations for the high state where $x_{1o} = 1943$ nM, $x_{2o} = 1891$ nM, $c_{1o} = 993$ nM, $c_{2o} = 966$ nM, $z_o = 40.9$ nM and $y_o = 1872$ nM. The time required for y (normalized between 0 and 1) to decay to half its maximum value was computed for each set of K_{D1} and K_{D2} values. In the single feedback loop models, the constitutive production rates of x_1 or x_2 (α_{1s} or α_{2s}) were set to 5 nM min^{-1} because this value approximated the Hill

functions at equilibrium for $u = 10$.

Strain name	Genotype
Wild-type (WT) P$_{GAL10}$Venus	MATa leu2, trp1::TRP1-P$_{GAL10}$Venus, ura3, ade2::ADE2, his3
GAL2Δ fb	MATa leu2::LEU2-P$_{TEFm4}$rtTA-M2, trp1::TRP1-P$_{GAL10}$Venus, ura3::URA3-P$_{TET}$GAL2, ade2::ADE2, his3, GAL2Δ::KAN
GAL3Δ fb	MATa leu2::LEU2-P$_{TEFm4}$rtTA-M2, trp1::TRP1-P$_{GAL10}$Venus, ura3::URA3-P$_{TET}$GAL3, ade2::ADE2, his3, GAL3Δ::KAN
GAL80Δ fb	MATa leu2::LEU2-P$_{TEFm4}$rtTA-M2, trp1::TRP1-P$_{GAL10}$Venus, ura3::URA3-P$_{TET}$GAL80, ade2::ADE2, his3, GAL80Δ::HPH
GAL2Δ fb GAL3Δ fb	MATa leu2::LEU2-P$_{TEFm4}$rtTA-M2, trp1::TRP1-P$_{GAL10}$Venus, ura3::URA3-P$_{TET}$GAL3, ade2::ADE2, his3::HIS3-P$_{ADH1}$GAL2, GAL3Δ::KAN, GAL2Δ::NAT
GAL2Δ fb GAL3Δ fb GAL80Δ fb	MATα ura3:URA3-P$_{TET}$GAL3, leu2::LEU2-P$_{STE5}$GAL80, ade2::ADE2-P$_{GAL10}$Venus, trp1::TRP1-P$_{ADH1}$GAL2, his3::HIS3-P$_{TEFm4}$rtTA-M2, GAL3Δ::KAN, GAL2Δ::NAT, GAL80Δ::HPH
GAL1Δ[†]	MATα leu2, trp1::TRP1-P$_{GAL10}$Venus, ura3, ade2::ADE2, his3, GAL1Δ
GAL1Δ[†] fb	MATα leu2::LEU2-P$_{TEFm4}$rtTA-M2, trp1::TRP1-P$_{GAL10}$Venus, ura3, ade2::ADE2, his3, GAL1Δ
GAL1Δ[†] GAL2Δ fb	MATα leu2::LEU2-P$_{TEFm4}$rtTA-M2, trp1::TRP1-P$_{GAL10}$Venus, ura3::URA3-P$_{TET}$GAL2, ade2::ADE2, his3, GAL2Δ::NAT, GAL1Δ
GAL1Δ[†] GAL3Δ fb	MATα leu2::LEU2-P$_{TEFm4}$rtTA-M2, trp1::TRP1-P$_{GAL10}$Venus, ura3::URA3-P$_{TET}$GAL3, ade2::ADE2, his3, GAL3Δ::KAN, GAL1Δ
GAL1Δ[†] GAL80Δ fb	MATα leu2::LEU2-P$_{TEFm4}$rtTA-M2, trp1::TRP1-P$_{GAL10}$Venus, ura3::URA3-P$_{TET}$GAL3, ade2::ADE2, his3, GAL80Δ::HPH, GAL1Δ
WT P$_{GAL3}$Venus	MATa leu2, trp1::TRP1-P$_{GAL3}$Venus, ura3, ade2::ADE2, his3
WT P$_{GAL80}$Venus	MATa leu2, trp1::TRP1-P$_{GAL80}$Venus, ura3, ade2::ADE2, his3
WT P$_{TDH3}$Venus	MATa leu2, trp1::TRP1-P$_{TDH3}$Venus, ura3, ade2::ADE2, his3
WT P$_{CYC1-G4BS}$Venus	MATa leu2, trp1::TRP1-P$_{CYC1-G4BS}$Venus, ura3, ade2::ADE2, his3
Wild-type diploid	MATa/α leu2/leu2::LEU2-P$_{TEFm4}$rtTA-M2, trp1::TRP1-P$_{GAL10}$Venus/trp1, ura3/ura3, ade2::ADE2/ade2, his3/his3
MA0182*	MATa/α, ura3/ura3::URA3-P$_{TETO2}$GAL3, his3::HIS3/his3, ade2::ADE2-P$_{MYO2}$rtTA/ade2::ADE2-P$_{GAL1}$YFP, GAL3Δ::KAN/GAL3Δ::KAN

Supplementary Table II: Strains used in this study. All strains were W303. [†]Constructed using CSY53 background described in [28]. *Strain described in [20].

Bibliography

[1] M Nakajima, K Imai, H Ito, T Nishiwaki, Y Murayama, H Iwasaki, T Oyama, and T Kondo. Reconstitution of circadian oscillation of cyanobacterial kaiC phosphorylation in vitro. *Science*, 308(5720):414–5, 2005.

[2] GM Suel, J Garcia-Ojalvo, LM Liberman, and MB Elowitz. An excitable gene regulatory circuit induces transient cellular differentiation. *Nature*, 440(7083):545–50, 2006.

[3] SM Block, JE Segall, and HC Berg. Adaptation kinetics in bacterial chemotaxis. *Journal of bacteriology*, 154(1):312–23, 1983.

[4] A Novick and M Weiner. Enzyme induction as an all-or-none phenomenon. *Proceedings of the National Academy of Sciences*, 43(7):553–66, 1957.

[5] IG de Jong, P Haccou, and OP Kuipers. Bet hedging or not? A guide to proper classification of microbial survival strategies. *Bioessays*, 33(3):215–23, 2011.

[6] H Maamar, A Raj, and D Dubnau. Noise in gene expression determines cell fate in *Bacillus subtilis*. *Science*, 317(5837):526–9, 2007.

[7] JW Veening, EJ Stewart, TW Berngruber, F Taddei, OP Kuipers, and LW Hamoen. Bet-hedging and epigenetic inheritance in bacterial cell development. *Proceedings of the National Academy of Sciences*, 105(11):4393–8, 2008.

[8] NQ Balaban, J Merrin, R Chait, L Kowalik, and S Leibler. Bacterial persistence as a phenotypic switch. *Science*, 305(5690):1622–5, 2004.

[9] SF Levy, N Ziv, and ML Siegal. Bet hedging in yeast by heterogeneous, age-correlated expression of a stress protectant. *PLoS Biology*, 10(5):e1001325, 2012.

[10] N Avraham, I Soifer, M Carmi, and N Barkai. Increasing population growth by asymmetric segregation of a limiting resource during cell division. *Molecular Systems Biology*, 9:656, 2013.

[11] MA Strauch, JJ Wu, RH Jonas, and JA Hoch. A positive feedback loop controls transcription of the spoOF gene, a component of the sporulation phosphorelay in *Bacillus subtilis*. *Molecular Microbiology*, 7(6):967–74, 1993.

[12] H Maamar and D Dubnau. Bistability in the *Bacillus subtilis* K-state (competence) system requires a positive feedback loop. *Molecular Microbiology*, 56(3):615–24, 2005.

[13] O Brandman and T Meyer. Feedback loops shape cellular signals in space and time. *Science*, 322(5900):390–395, 2008.

[14] KJ Aström and RM Murray. *Feedback Systems: An Introduction for Scientists and Engineers*. Princeton University Press, 2008.

[15] N Rosenfeld, MB Elowitz, and U Alon. Negative autoregulation speeds the response time of transcription networks. *Journal of Molecular Biology*, 323(5):785–793, 2002.

[16] A Becskei and L Serrano. Engineering stability in gene networks by autoregulation. *Nature*, 405:590–593, 2000.

[17] L Ashall, CA Horton, DE Nelson, P Paszek, CV Harper, K Sillitoe, S Ryan, DG Spiller, JF Unitt, DS Broomhead, DB Kell, DA Rand, V See, and MR White. Pulsatile stimulation determines timing and specificity of NF-kappaB-dependent transcription. *Science*, 324(5924):242–6, 2009.

[18] SR Biggar and GR Crabtree. Cell signaling can direct either binary or graded transcriptional responses. *The EMBO Journal*, 20(12):3167–76, 2001.

[19] OS Venturelli, H El-Samad, and RM Murray. Synergistic dual positive feedback loops established by molecular sequestration generate robust bimodal response. *Proceedings of the National Academy of Sciences*, 109(48), 2012.

[20] M Acar, A Becskei, and A Oudenaarden. Enhancement of cellular memory by reducing stochastic transitions. *Nature*, 435:228–232, 2005.

[21] FJ Isaacs, J Hasty, CR Cantor, and JJ Collins. Prediction and measurement of an autoregulatory genetic module. *Proceedings of the National Academy of Sciences*, 100(13):7714–7719, 2003.

[22] TE Torchia, RW Hamilton, CL Cano, and JE Hopper. Disruption of regulatory gene GAL80 in *Saccharomyces cerevisiae*: effects on carbon-controlled regulation of the galactose/melibiose pathway genes. *Molecular Cellular Biology*, 4(8):1521–7, 1984.

[23] JF Tschopp, SD Emr, C Field, and R Schekman. GAL2 codes for a membrane-bound subunit of the galactose permease in *S*accharomyces cerevisiae.

[24] TE Torchia and JE Hopper. Genetic and molecular analysis of the GAL3 gene in the expression of the galactose/melibiose regulon of *Saccharomyces cerevisiae*. *Genetics*, 113(2):229–46, 1986.

[25] P Bhat and J Hopper. Overproduction of the GAL1 or GAL3 protein causes galactose-independent activation of the GAL4 protein: evidence for a new model of induction for the yeast GAL/MEL regulon. *Molecular Cell Biology*, 12(6):2701–2707, 1992.

[26] DJ Timson, HC Ross, and RJ Reece. Gal3p and Gal1p interact with the transcriptional repressor Gal80p to form a complex of 1:1 stoichiometry. *Biochemistry Journal*, 363(Pt 3):515–20, 2002.

[27] W Bajwa, TE Torchia, and JE Hopper. Yeast regulatory gene GAL3: carbon regulation; UASGal elements in common with GAL1, GAL2, GAL7, GAL10, GAL80, and MEL1; encoded protein strikingly similar to yeast and *Escherichia coli galactokinases*, journal = Molecular Cellular Biology, volume = 8, number = 8, pages = 3439-47, year = 1988.

[28] MK Hawkins and CD Smolke. The regulatory roles of the galactose permease and kinase in the induction response of the GAL network in *Saccharomyces cerevisae*. *Journal of Biological Chemistry*, 281(19):13485–13492, 2006.

[29] CA Sellick, TA Jowitt, and RJ Reece. The effect of ligand binding on the galactokinase activity of yeast Gal1p and its ability to activate transcription. *Journal of Biological Chemistry*, 284(1):229–36, 2009.

[30] JB Thoden, CA Sellick, DJ Timson, RJ Reece, and HM Holden. Molecular structure of *Saccharomyces cerevisiae* Gal1p, a bifunctional galactokinase and transcriptional inducer. *Journal of Biological Chemistry*, 280(44):36905–11, 2005.

[31] TC Hittinger and SB Carroll. Gene duplication and the adaptive evolution of a classic genetic switch. *Nature*, 449:677–681, 2007.

[32] M Johnston. A model fungal gene regulatory mechanism: the GAL genes of *Saccharomyces cerevisiae*. *Microbiological Reviews*, 51(4):458–476, 1987.

[33] I Zacharloudakis, T Gligoris, and D Tzamarias. A yeast catabolic enzyme controls transcriptional memory. *Current Biology*, 17(23):2041–2046, 2007.

[34] D Abramczyk, S Holden, CJ Page, and RJ Reece. Interplay of a ligand sensor and an enzyme in controlling expression of the *Saccharomyces cerevisiae* GAL genes. *Eukaryotic Cell*, 11(3):334–42, 2011.

[35] MN Artyomov, J Das, M Kardar, and A Chakraborty. Purely stochastic binary decisions in cell signaling models without underlying deterministic bistabilities. *Proceedings of the National Academy of Sciences*, 104(48):18958–18963, 2007.

[36] M Samoilov, S Plyasunov, and A Arkin. Stochastic amplification and signaling in enzymatic futile cycles through noise-induced bistability with oscillations. *Proceedings of the National Academy of Sciences*, 102(7):2310–2315, 2005.

[37] TB Kepler and TC Elston. Stochasticity in transcriptional regulation: origins, consequences and mathematical representations. *Biophysical Journal*, 81(6):3116–3136, 2001.

[38] I Lestas, J Paulsson, NE Ross, and G Vinnicombe. Noise in gene regulatory networks. *Automatic Control, IEEE Transactions*, 53(Special issue on systems biology):189–200, 2008.

[39] GM Guidi and A Goldbeter. Bistability without hysteresis in chemical reaction systems: A theoretical analysis of irreversible transitions between multiple steady states. *Journal of Physical Chemistry*, 101:9367–9376, 1997.

[40] T Nagai, K Ibata, ES Park, M Kubota, K Mikoshiba, and A Miyawaki. A variant of yellow fluorescent protein with fast and efficient maturation for cell-biological applications. *Nature Biotechnology*, 20(1):87–90, 2002.

[41] HC Douglas and DC Hawthorne. Enzymatic expression and genetic linkage of genes controlling galactose utilization in *Saccharomyces*. *Genetics*, 49:837–44, 1964.

[42] MI Riley and RC Dickson. Genetic and biochemical characterization of the galactose gene cluster in *Kluyveromyces lactis*. *Journal of bacteriology*, 158(2):705–12, 1984.

[43] S Urlinger, U Baron, M Thellmann, MT Hasan, H Bujard, and W Hillen. Exploring the sequence space for tetracycline-dependent transcriptional activators: novel mutations yield expanded range and sensitivity. *Proceedings of the National Academy of Sciences of the United States of America*, 97(14):7963–8, 2000.

[44] D Angeli, JE Ferrell, and ED Sontag. Detection of multistability, bifurcations, and hysteresis in a large class of biological positive-feedback systems. *Proceedings of the National Academy of Sciences of the United States of America*, 101(7):1822–7, 2004.

[45] RL Iman, JM Davenport, and DK Zeigler. Latin hypercube sampling program users guide. *Technical Report Sandia Labs*, 1980.

[46] Jr. Ferrell, JE. Tripping the switch fantastic: how a protein kinase cascade can convert graded inputs into switch-like outputs. *Trends Biochemical Sciences*, 21(12):460–6, 1996.

[47] NE Buchler and M Louis. Molecular titration and ultrasensitivity in regulatory networks. *Journal of Molecular Biology*, 384(5):1106–19, 2008.

[48] NE Buchler and FR Cross. Protein sequestration generates a flexible ultrasensitive response in a genetic network. *Molecular Systems Biology*, 5:272, 2009.

[49] SY Kim and Jr Ferrell, JE. Substrate competition as a source of ultrasensitivity in the inactivation of Wee1. *Cell*, 128(6):1133–45, 2007.

[50] Jr Ferrell, JE. Feedback regulation of opposing enzymes generates robust, all-or-none bistable responses. *Current Biology*, 18(6):R244–5, 2008.

[51] MJ Dunlop, RS Cox, JH Levine, RM Murray, and MB Elowitz. Regulatory activity revealed by dynamic correlations in gene expression noise. *Nature Genetics*, 40(12):1493–8, 2008.

[52] CD Thron. A model for a bistable biochemical trigger of mitosis. *Biophysical Chemistry*, 57(2-3):239–51, 1996.

[53] Jr Ferrell, JE. Self-perpetuating states in signal transduction: positive feedback, double-negative feedback and bistability. *Current Opinion in Cell Biology*, 14(2):140–8, 2002.

[54] CV Cabrera, MC Alonso, and H Huikeshoven. Regulation of scute function by extramacrochaete in vitro and in vivo. *Development*, 120(12):3595–603, 1994.

[55] A Bhattacharya and NE Baker. A network of broadly expressed HLH genes regulates tissue-specific cell fates. *Cell*, 147(4):881–92, 2011.

[56] M Van Doren, HM Ellis, and JW Posakony. The *Drosophila* extramacrochaetae protein antagonizes sequence-specific DNA binding by daughterless/achaete-scute protein complexes. *Development*, 113(1):245–55, 1991.

[57] JW Veening, WK Smits, and OP Kuipers. Bistability, epigenetics, and bet-hedging in bacteria. *Annual Reviews Microbiology*, 62:193–210, 2008.

[58] T Pfeiffer and S Bonhoeffer. Evolution of cross-feeding in microbial populations. *The American Naturalist*, 163(6), 2004.

[59] E Nevoigt, J Kohnke, CR Fischer, H Alper, U Stahl, and G Stephanopoulos. Engineering of promoter replacement cassettes for fine-tuning of gene expression in *Saccharomyces cerevisiae*. *Applied Environmental Microbiology*, 72(8):5266–73, 2006.

[60] R Lutz and H Bujard. Independent and tight regulation of transcriptional units in *Escherichia coli* via the LacR/O, the TetR/O and AraC/I1-I2 regulatory elements. *Nucleic Acids Research*, 25(6):1203–10, 1997.

[61] CM Bishop. *Pattern recognition and machine learning*. Springer, 2006.

[62] KJ Livak and TD Schmittgen. Analysis of relative gene expression data using real-time quantitative PCR and the $2^{-\Delta\Delta C_t}$ method. *Methods*, 25:402–408, 2001.

[63] MA Teste, M Duquenne, JM Francois, and JL Parrou. Validation of reference genes for quantitative expression analysis by real-time RT-PCR in *Saccharomyces cerevisiae*. *BMC Molecular Biology*, 10:99, 2009.

[64] A Dickenstein and IZ Emiris. *Solving Polynomial Equations: Foundations, Algorithms, and Applications (Algorithms and Computation in Mathematics)*. Springer, 2005.

[65] C Mateus and SV Avery. Destabilized green fluorescent protein for monitoring dynamic changes in yeast gene expression with flow cytometry. *Yeast*, 16(14):1313–23, 2000.

[66] WK Huh, JV Falvo, LC Gerke, AS Carroll, RW Howson, JS Weissman, and EK O'Shea. Global analysis of protein localization in budding yeast. *Nature*, 425(6959):686–91, 2003.

[67] CB Tyson, PG Lord, and AE Wheals. Dependency of size of *Saccharomyces cerevisiae* cells on growth rate. *Journal of bacteriology*, 138(1):92–8, 1979.

[68] JR Newman, S Ghaemmaghami, J Ihmels, DK Breslow, M Noble, JL DeRisi, and JS Weissman. Single-cell proteomic analysis of *S. cerevisiae* reveals the architecture of biological noise. *Nature*, 441(7095):840–6, 2006.

[69] MA Savageau. *Biochemical Systems Analysis*. Addison-Wesley Publishing Company, 1976.

[70] G Peng and JE Hopper. Evidence for Gal3p's cytoplasmic location and Gal80p's dual cytoplasmic-nuclear location implicates new mechanisms for controlling Gal4p activity in *Saccharomyces cerevisiae. Molecular Cellular Biology*, 20(14):5140–8, 2000.

[71] R Wightman, R Bell, and RJ Reece. Localization and interaction of the proteins constituting the GAL genetic switch in *Saccharomyces cerevisiae. Eukaryotic Cell*, 7(12):2061–8, 2008.

[72] O Egriboz, F Jiang, and JE Hopper. Rapid GAL gene switch of *Saccharomyces cerevisiae* depends on nuclear Gal3, not nucleocytoplasmic trafficking of Gal3 and Gal80. *Genetics*, 189(3):825–36, 2011.

[73] M Hong, MX Fitzgerald, S Harper, C Luo, DW Speicher, and R Marmorstein. Structural basis for dimerization in DNA recognition by Gal4. *Structure*, 16(7):1019–26, 2008.

[74] V Pilauri, M Bewley, C Diep, and J Hopper. Gal80 dimerization and the yeast GAL gene switch. *Genetics*, 169(4):1903–14, 2005.

[75] K Melcher and E Xu. Gal80-Gal80 interaction on adjacent Gal4p binding sites is required for complete GAL gene repression. *The EMBO Journal*, 20:841–851, 2001.

[76] E Giniger and M Ptashne. Cooperative DNA binding of the yeast transcriptional activator GAL4. *Proceedings of the National Academy of Sciences*, 85(2):382–6, 1988.

[77] DW Griggs and M Johnston. Promoter elements determining weak expression of the GAL4 regulatory gene of *Saccharomyces cerevisiae. Molecular Cell Biology*, 13(8):4999–5009, 1993.